Available online at www.sciencedirect.com
ScienceDirect
Geochimica et Cosmochimica Acta 74 (2010) 41–58
Geochimica et Cosmochimica Acta
www.elsevier.com/locate/gca

Nanoparticles in natural systems I: The effective reactive surface area of the natural oxide fraction in field samples

Tjisse Hiemstra [a,*], Juan Antelo [a,1], Rasoul Rahnemaie [b], Willem H. van Riemsdijk [a]

[a] Department of Soil Quality, Wageningen University, P.O. Box 47, NL 6700 AA Wageningen, The Netherlands
[b] Department of Soil Science, Tarbiat Modares University, P.O. Box 14115-336, Tehran, Iran

Received 19 March 2009; accepted in revised form 18 September 2009; available online 14 October 2009

Abstract

Information on the particle size and reactive surface area of natural samples is essential for the application of surface complexation models (SCM) to predict bioavailability, toxicity, and transport of elements in the natural environment. In addition, this information will be of great help to enlighten views on the formation, stability, and structure of nanoparticle associations of natural organic matter (NOM) and natural oxide particles.

Phosphate is proposed as a natively present probe ion to derive the effective reactive surface area of natural samples. In the suggested method, natural samples are equilibrated ($\geqslant 10$ days) with 0.5 M $NaHCO_3$ (pH = 8.5) at various solid–solution ratios. This matrix fixes the pH and ionic strength, suppresses the influence of Ca^{2+} and Mg^{2+} ions by precipitation these in solid carbonates, and removes NOM due to the addition of activated carbon in excess, collectively leading to the dominance of the PO_4–CO_3 interaction in the system. The data have been interpreted with the charge distribution (CD) model, calibrated for goethite, and the analysis results in an effective reactive surface area (SA) and a reversibly bound phosphate loading Γ for a series of top soils.

The oxidic SA varies between about 3–30 m^2/g sample for a large series of representative agricultural top soils. Scaling of our data to the total iron and aluminum oxide content (dithionite–citrate–bicarbonate extractable), results in the specific surface area between about 200–1200 m^2/g oxide for most soils, i.e. the oxide particles are nano-sized with an equivalent diameter in the order of ~1–10 nm if considered as non-porous spheres. For the top soils, the effective surface area and the soil organic carbon fraction are strongly correlated. The oxide particles are embedded in a matrix of organic carbon (OC), equivalent to $\sim 1.4 \pm 0.2$ mg OC/m^2 oxide for many soils of the collection, forming a NOM–mineral nanoparticle association with an average NOM volume fraction of ~80%. The average mass density of such a NOM–mineral association is $\sim 1700 \pm 100$ kg/m^3 (i.e. high-density NOM). The amount of reversibly bound phosphate is rather close to the amount of phosphate that is extractable with oxalate. The phosphate loading varies remarkably ($\Gamma \approx$ 1–3 μmol/m^2 oxide) in the samples. As discussed in part II of this paper series (Hiemstra et al., 2010), the phosphate loading (Γ) of field samples is suppressed by surface complexation of NOM, where hydrophilic, fulvic, and humic acids act as a competitor for (an)ions via site competition and electrostatic interaction.

1. INTRODUCTION

The bioavailability as well as mobility of ions largely depends on the interaction with organic matter and mineral particles. The interaction is a complex process, often involving much more than a simple adsorption reaction or ion exchange. Factors such as pH, ionic strength, the presence of competing or promoting ions as well as the nature and the amount of substrate, all affect the distribution of cat- and anions over the solid and solution phase.

Our understanding of the binding of ions to well-defined mineral particles has increased in the last decade because of the development of in-situ surface spectroscopy and surface

* Corresponding author.
E-mail address: tjisse.hiemstra@wur.nl (T. Hiemstra).
[1] Present address: Department of Physical Chemistry, Santiago de Compostela University, Av. de las Ciencias s/n 15782, Spain.

0016-7037/$ - see front matter © 2009 Elsevier Ltd. All rights reserved.
doi:10.1016/j.gca.2009.10.018

complexation models (SCM). Ideally, SCM may predict changes in situations where experimental data are not available or difficult to collect. Surface complexation models have widely been used to estimate the distribution of metal- and oxyanions between solution and mineral surfaces (Ali and Dzombak, 1996; Antelo et al., 2005; Boily, 1999; Christl and Kretzschmar, 1999; Criscenti and Sverjensky, 1999; Davis and Leckie, 1978; Dzombak and Morel, 1990; Hiemstra and Van Riemsdijk, 1996; Lutzenkirchen, 2004; Ponthieu et al., 2006; Tadanier and Eick, 2002).

In general, the application of SCM to natural systems like soils, sediments, and other aquatic media is quite complicated. Natural systems are usually complex, containing many different elements that may interact with a number of mineral particles. Two important complications related to the application of SCM to field samples are "how to derive the reactive surface area of the oxide fraction?" and "how to deal with the interaction of natural organic matter with oxide particles?" Both aspects need our attention at priority. In part I of this paper series, we discuss the determination of the effective surface area of the natural oxide fraction in field samples. In part II (Hiemstra et al., 2010), the effective NOM loading of the natural oxide fraction will be assessed. Both are required to apply surface complexation modeling to field samples. These are also of great interest to enlighten views on the formation, stability, and structure of nanoparticle associations of natural organic matter (NOM) and natural oxide particles.

Any application of electrostatic SCM's to natural systems requires in the first place information about the reactive surface area of the material involved in the adsorption process. Most SCM use an electrostatic module with a diffuse double layer (DDL) to calculate the interaction energy between ions that are adsorbed at the charged surface. The corresponding theory uses the electric field strength that represents the charge per unit surface area (C/m^2). Various approaches can be followed to incorporate a reactive surface area in a SCM.

(A) The classical method of gas adsorption, i.e. BET method, has been used to measure the reactive surface area of natural sands (Logue et al., 2004; Rosentreter et al., 1998). A disadvantage is that natural materials are often heterogeneous, in which part of the measured surface area (A in m^2/kg material) may be not reactive in the adsorption process that is considered. For instance, clay minerals may be present, while the focus is on the oxide fraction. It is also possible that adsorbed natural organic matter (NOM) may mask part of the mineral surface area (Kaiser and Guggenberger, 2000, 2003). The BET surface of natural ferrihydrites (Schwertmann and Fischer, 1973) as well as synthetic oxides (Eusterhues et al., 2003; Kaiser and Guggenberger, 2000; Mödl et al., 2007) are negatively correlated with the NOM content. To reduce this effect, one may try to remove the organic matter (Kaiser and Guggenberger, 2003; Mayer, 1994; Wagai et al., 2009). In addition, one may remove the oxide fraction(s) and estimate from the difference the contribution(s) (Eusterhues et al., 2005). In the latter procedure, the surface area with oxidic properties present at the edges of clay particles may not be included and measuring a surface area with a method-by-difference may lead to large uncertainties. Moreover, the oxidation of organic matter may change the remaining mineral particles (Mayer, 1994). Another point is the strong dehydration that is part of the BET measurement. This may decrease irreversibly the surface area because small particles in the dry state may have a high area of contact, as found for the nano-colloids of synthetic ferrihydrite (Davis and Leckie, 1978; Dzombak and Morel, 1990). An alternative approach is the use of ethylene glycol monoethyl ether (EGME) as probe molecule (Cihacek and Bremner, 1979) but this conventional method typically measures the surface area of clay mineral fraction (Kennedy et al., 2002) which includes in particular the surface area of the basal planes. From this perspective, the use of an EGME surface area is problematic if the surface complexation of anions is to be evaluated. Nevertheless, it has been used for scaling MoO_4^{2-} adsorption of soils (Goldberg et al., 2002), illustrating the urge for development of better methods.

(B) Focusing on iron and aluminum (hydr)oxides in a natural sample, another approach is to measure the amount of reactive solid phase(s) by selective dissolution, and attribute an assumed specific surface area (SSA in m^2/g oxide) to the constituent dissolved (Cances et al., 2003; Dijkstra et al., 2004; Eusterhues et al., 2005; Gustafsson, 2001; Lofts and Tipping, 1998; Lumsdon, 2004; Schroder et al., 2005; Weng et al., 2001). The first step in the procedure is the determination of the iron and aluminum (hydr)oxide content of a soil or aquifer material. Extraction with dithionite–citrate–bicarbonate (DCB) (Mehra and Jackson, 1960) is considered to represent the total iron (hydr)oxide content. The most reactive part of the natural (hydr)oxide fraction is usually characterized by the extraction of Fe and Al with acid ammonium oxalate (Roden and Zachara, 1996; Schwertmann, 1973) or a bicarbonate–citrate–ascorbate (pH = 8) mixture (Kostka and Luther, 1994; Meima and Comans, 1998). The oxalate extraction is catalyzed by Fe(II) ions and therefore may include Fe(II)/Fe(III) minerals like magnetite (Fe_3O_4) if present (Kostka and Luther, 1994), whereas this is suppressed or avoided when using ascorbate. The next step in the procedure is transforming the extracted amount of Fe and Al into a corresponding surface area. The specific surface area of the most reactive Fe oxide fraction is usually set equal to the specific surface area of 2-line ferrihydrite (Davis et al., 1978; Dzombak and Morel, 1990) but may also refer to particles with less surface area such as nanogoethite (Thompson et al., 2006; van der Zee et al., 2003). For the Al fraction, a very high surface area has been assumed (Dijkstra et al., 2004; Gustafsson, 2001). Assumed is the presence of gibbsite but this Al fraction can also be due to the presence of phyllosilicates (Wiseman and Puttmann, 2006) and other silicates like allophane (Gustafsson, 2001). The Fe–DCB extraction will include the crystalline Fe oxide fraction of natural materials, which may have a considerably smaller surface area than ferrihydrite, for instance a difference of a factor 10. Nevertheless, its contribution may be important because the DCB fraction can be relatively large in certain samples. In top soils, the difference between the Fe fraction extracted with oxalate and total iron (DCB) may be not very large, while in sub soils the difference may be a factor of about 3 to even 10 (Weng et al., 2001).

(C) A third approach to derive the surface area uses SCM with a set of adsorption constants derived for a reference material (representative metal oxide). The method derives the reactive surface area that is needed to explain the experimental adsorption of a natural material with the chosen set of parameters. If adsorption data of heavy metals are used, the major disadvantage is that the metal-ion binding in the soil material can easily be dominated by the organic fraction and ion exchange (Voegelin et al., 2001; Weng et al., 2001). To assess a realistic reactive surface area for metal oxides, we consider the use of an anion as a probe molecule as the most adequate choice.

In the present paper, a method is discussed that uses a well-chosen probe anion to estimate the effective reactive oxide surface area of natural samples. The distribution of the anion over the solid and solution phase is determined and interpreted using separately determined binding properties of the probe anion for a representative oxide mineral, yielding an effective reactive surface area. The term "effective" is used since it is assumed that the behavior of the natural (hydr)oxide fraction can be represented by a model oxide. A rational is that the collective behavior is strongly dominated by electrostatic properties, which are, in a first order approach, rather similar for the various oxides of iron and aluminum. For the model oxide, we have chosen goethite because it is an important iron (hydr)oxide identified in many natural systems (Cornell and Schwertmann, 1996; Thompson et al., 2006; van der Zee et al., 2003), and an extensive database is available for ion adsorption on goethite derived for the charge distribution (CD) model (Hiemstra and Van Riemsdijk, 1996). Ferrihydrite can be considered as a good or even better alternative. However, a corresponding database for ferrihydrite is not available yet, although a first step in this direction has recently been made (Hiemstra and Van Riemsdijk, 2009). The chosen probe ion is phosphate, since it binds predominantly to metal oxide surfaces. Moreover, phosphate is omnipresent in natural systems in relevant amounts, even if the solution concentration is very low, and its behavior has been studied extensively in literature. To approach the effective reactive surface area successfully, it is essential that the surface complexation model can predict the phosphate adsorption behavior in natural systems. This requires well-defined conditions.

Natural systems are multi-component systems. It implies that many interactions can influence the distribution of an ion over the solid and solution phase. The adsorption of phosphate is influenced by the major cations (Na^+, K^+, Ca^{2+}, Mg^{2+}, Al^{3+}) and major inorganic anions (HCO_3^-, Cl^-, NO_3^-, SO_4^{2-}) of the natural aqueous solution. Ideally, the complicated solution matrix is replaced by a simpler set of solution conditions that minimizes the number of relevant interactions.

In many phosphate extraction methods, ions are added in high concentrations to compete with the phosphate ions adsorbed to natural particles. Electrolytic, acidic, or basic solutions are added to desorb the readily extractable phosphate fraction from soil samples. An inspiring method is based on the carbonate ion as competitor (Olsen et al., 1954). A solution with a high concentration of $NaHCO_3$ (0.5 M), adjusted to pH 8.5, is used. The added solution will buffer the pH and fix the ionic strength. The created conditions stimulate the phosphate desorption process due to (a) the relatively high pH value of the extraction solution and (b) the competitive binding of carbonate ions (Rahnemaie et al., 2007a). In addition (c), the added (bi)carbonate will reduce the concentration of Ca^{2+} and Mg^{2+} due to precipitation of these ions in solid carbonates. Ca^{2+} and Mg^{2+} ions act cooperative in the phosphate binding when adsorbed (Rietra et al., 2001; Stachowicz et al., 2008). For the conditions of the extraction, a large part of the natural organic matter (NOM) fraction will dissolve and is removed in the procedure by adding a large excess of activated carbon. Overall, the triple action (a–c) of the 0.5 M $NaHCO_3$ solution in combination with the presence of activated carbon creates conditions that enable a more accurate calculation of the phosphate–oxide interaction.

The aim of this study is to determine the effective reactive surface area of the metal oxide fraction of natural materials and this is the beginning rather than the end of a journey. A series of equilibrations of a soil with $NaHCO_3$ solutions will be carried out for a set of different samples. The competitive phosphate–carbonate ad/desorption process in the samples will be interpreted with the charge distribution model (Hiemstra and Van Riemsdijk, 1996), yielding an effective surface area.

With the above approach, for the first time, a procedure is developed that determines for natural samples the effective reactive oxide surface area. This information will be applied in part II (Hiemstra et al., 2010) to analyze the effect of the presence of NOM at the surface of natural oxide particles under standardized field conditions, for fertilized top soils simulated by a 0.01 M $CaCl_2$ background electrolyte solution (van Erp et al., 1998). This will result in the calculation of an effective NOM density. The combination of determining an effective surface area of oxide particles and an effective NOM density will enable a consistent scaling of SCM to field samples conditions.

2. MATERIALS AND METHODS

2.1. Soils samples

From a large collection of representative agricultural top soils of the Netherlands, known as the Copernicus Series (van Erp et al., 1998), a subset was chosen. A number of general characteristics of this selection are shown in Table 1. As follows from Table 1, the soil samples cover a wide range of organic carbon contents (~1–15% OC), clay contents (~3–30%), pH values (~4–7), DOC (~5–70 mg/L), and aqueous soluble orthophosphate concentrations (~1–30 μM).

2.2. Natural oxide fraction

The general set of soil characteristics (Table 1) has been extended with ammonium oxalate extractions to determine the Fe and Al oxide fraction that is strongly related to the smallest particles (Roden and Zachara, 1996; Schwertmann, 1973). The soils were extracted with 0.2 M

Table 1
Soil characteristics of the Copernicus series

Soil[a]	OC[b] (%)	<2 μm (%)	Fe-ox [c] (mmol/kg)	Al-ox [c]	P-ox [c]	Fe–DCB [d]	Al–DCB [d]	pH [e]	DOC [e] (mgC/L)	Na^{+} [e] (mM)	K^{+} [e] (mM)	Mg^{2+} [e] (mM)	Ca^{2+} [e] (mM)	$P–PO_4$ [e] (μM)	R_{ev} [f] (mmol/kg)	A [f] (m^2/g soil)	FeNOM [g] (μmol m^{-2})
1	1.8	5	32.4	34.4	19.6	48	41	4.3	11.6	0.0	0.3	0.3	9.6	30.0	23.0 ± 0.4	11.3 ± 0.3	1.07 ± 0.04
2	2.2	7	48.5	32.6	22.7	119	39	5.2	19.6	1.2	9.1	0.6	9.3	17.7	27.3 ± 4.6	14.9 ± 3.0	1.46 ± 0.17
3	3.7	8	342.2	18.6	38.2	852	27	5.6	16.2	0.7	4.1	1.2	8.9	1.6	50.4 ± 6.0	32.7 ± 4.7	1.27 ± 0.11
4	3.3	11	92.7	32.7	31.5	125	34	5.6	13.7	1.4	7.2	0.8	9.3	6.8	55.4 ± 3.4	34.0 ± 2.3	1.54 ± 0.00
5	1.3	15	75.7	20.2	14.9	168	30	4.9	19.5	0.5	1.2	0.5	9.5	2.3	9.3 ± 0.2	5.0 ± 0.1	0.72 ± 0.04
6	1.5	9	42.9	16.4	8.6	68	25	5.0	12.6	0.2	1.8	0.4	9.7	1.9	5.3 ± 0.5	3.1 ± 0.4	0.96 ± 0.19
7	0.9	11	50.3	19.1	14.9	135	27	5.7	8.7	0.5	2.1	0.3	10.0	17.1	14.3 ± 2.2	6.6 ± 1.4	1.12 ± 0.40
8	3.0	14	95.9	31.1	18.8	101	32	5.0	26.6	0.7	3.3	0.7	9.4	1.6	15.7 ± 1.2	10.8 ± 0.9	0.83 ± 0.04
9	4.9	21	211.3	27.5	34.9	242	36	4.6	37	2.4	5.3	1.0	8.8	2.6	41.2 ± 0.6	27.3 ± 0.5	1.23 ± 0.00
10	8.3	25	252.2	46.2	25.7	318	59	4.9	32	1.0	2.2	0.7	9.4	0.6	21.9 ± 1.7	18.9 ± 1.5	1.48 ± 0.01
11	14.0	28	131.7	57.7	20.3	146	n.d.	5.5	71.7	2.1	5.5	2.3	8.2	2.9	19.4 ± 1.5	15.2 ± 1.3	1.94 ± 0.03
12	3.3	13	114.4	20.9	30.2	233	29	4.5	23.9	1.3	11.2	0.9	9.0	27.1	42.1 ± 1.5	23.3 ± 1.0	1.37 ± 0.02
13	1.8	26	64.8	32.2	14.0	178	32	7.2	13.8	1.2	1.4	0.4	10.1	2.3	9.1 ± 0.8	4.5 ± 0.6	0.62 ± 0.27
14	0.6	3	10.5	3.0	7.8	16	6	6.8	4.9	0.3	2.4	0.2	10.1	17.1	9.5 ± 0.6	3.4 ± 0.4	0.41 ± 0.44
15	4.1	28	117.1	38.9	24.0	200	30	6.4	17.7	1.1	3.6	0.8	9.5	5.8	18.7 ± 1.5	9.8 ± 1.0	1.29 ± 0.13
16	1.0	6	31.4	23.7	15.6	84	34	6.0	6	0.1	3.2	0.2	10.1	9.4	11.3 ± 0.5	5.2 ± 0.3	1.01 ± 0.13
17	2.9	12	115.7	29.4	40.2	277	32	7.1	12.5	0.5	3.9	0.5	10.0	23.9	47.0 ± 6.2	23.0 ± 3.7	1.41 ± 0.15
18	2.1	12	67.8	28.8	19.3	116	36	5.6	17.5	1.2	3.1	0.5	10.4	4.2	21.9 ± 1.4	13.6 ± 1.0	1.53 ± 0.04
19	1.6	17	42.4	29.9	11.2	153	59	6.3	12	0.4	0.7	0.3	10.3	4.2	8.3 ± 0.7	4.4 ± 0.5	1.22 ± 0.21

[a] Soils with numbers in bold were selected to study of the rate of equilibration.
[b] Organic carbon according to Kurmies.
[c] Two hours extraction (solid–solution ratio SSR = 0.05 g/L) with 0.2 M oxalate (pH = 3.0), see text.
[d] Based on Holmgren (1967), see text. n.d. = not determined. The average amount of Al^{3+} bound by the CEC is about 4 ± 3 mmol/kg, which is ~10% of the amount of Al extracted with oxalate or DCB. At precipitation, this amount of Al^{3+} will probably not contribute much to the formation of new surface area.
[e] Measured in a 0.01 M $CaCl_2$ extract (solid-solution ratio SSR = 0.1 kg/L, time = 2 h, van Erp et al. (1998)).
[f] Fitted using the 0.5 M $NaHCO_3$ equilibrium data.
[g] Effective NOM loading calculated in order to explain the PO_4 concentration in 0.01 M $CaCl_2$ based on the R_{ev} and A derived from 0.5 M HCO_3 equilibration (Hiemstra et al., 2010).

oxalate of pH = 3.00, i.e. 16.2 g $(COONH_4)_2.H_2O$ with 10.9 g $(COOH)_2.2H_2O$ per liter, for 2 h in the dark at 22 ± 1 °C using a solid–solution ratio (SSR) of 0.05 kg soil/L. The selected soils differ by a factor 10 in the measured Fe and Al contents (Table 1). In almost all soils, oxalate extractable Fe is somewhat higher than the extractable Al. In addition, dithionite–citrate–bicarbonate (DCB) extractions were done to determine the total Fe oxide fraction. Aluminum was also measured in these extracts. Comparing Fe extracted with oxalate and DCB shows that on average the Fe–DCB fraction is about 1.4 times larger, which has previously also been found for other Dutch top soils (Weng et al., 2001). According to Wada (1989), the DCB treatment is thought to extract the same components as the oxalate extraction with the exception of allophane and imogolite, but it extracts in addition crystalline oxyhydroxides of Fe. Sodium dithionite is a strong reducing agent that solubilizes secondary iron (hydr)oxides, including goethite, hematite, and maghemite. Normally, the reductant-ligand-buffer behavior of the DCB extraction is increased by heating the solution to 70–80 °C, but also dithionite is capable dissolving the crystalline Fe oxides at room temperature in overnight extractions employing a higher citrate concentration (Holmgren, 1967). In the present study, we carried out the dithionite extraction with the bicarbonate buffer solution using the following procedure: a volume of 30 mL of a solution of 0.66 M citrate and 0.11 M sodium bicarbonate was added to polyethylene tubes containing 0.30 g of soil sample. Sodium dithionite (0.64 g) was added to each tube, and the suspensions were shaken overnight (~16 h). Next, the samples were centrifuged and the supernatants were removed and stored for Fe and Al analysis. Dissolved Fe, Al, and/or P concentrations in the different extracts were measured by inductively coupled plasma atomic emission spectroscopy (ICP-AES). Blanks with the buffer solution were prepared and the analyses were duplicated in all cases. All extraction experiments were carried out in polyethylene labware to avoid silica contamination, and the temperature was maintained at 22 ± 1 °C in a constant temperature room.

2.3. Phosphate desorption

The competitive desorption method for phosphate that was used in this study is based on the phosphate extraction method with bicarbonate used by Barrow and Shaw (1976a, 1976b). The phosphate desorption has been carried out by adding a freshly prepared 0.50 M $Na(H)CO_3$ solution (pH 8.5) to soils creating different solid–solution ratios (SSR).

The 0.50 M $Na(H)CO_3$ solution was freshly prepared by dissolving 42.4 g $NaHCO_3$ (Merck PA) per liter. The pH of this solution has been adjusted to pH 8.50 by pipetting about 8–10 mL/L of a 2 M NaOH solution (8 g NaOH/100 mL). A set of commercial buffers of pH 7 and pH 9 or 10 was used to calibrate the pH meter used. Note that the extraction solution is supersaturated with respect to atmospheric CO_2 and significant escape of CO_2 should be prevented.

For each soil, a series with a solid–solution ratio (SSR) of 1/5, 1/20, 1/50, 1/100, 1/200, and 1/300 kg/L was prepared by adding x g air-dry soil to y mL 0.50 M $Na(H)CO_3$ solution in low-density polyethylene bottles according to x g/y mL = 2.0 g soil/10 mL (50 mL bottle), 1.0 g/20 mL (50 mL bottle), 1.0 g/50 mL (100 mL bottle), 1.0 g/100 mL (100 mL bottle), 1.0 g/200 mL (250 mL bottle), and 0.5 g/150 mL (250 mL bottle). To suppress or remove the competitive interaction of NOM, 0.40 g of activated carbon (Merck PA) per gram of soil sample was added to the suspensions. It turned out that this activated carbon contained unfortunately some phosphate soluble in 0.5 M $Na(H)CO_3$. Therefore, the calculated phosphate loading was later corrected (<2–5%) for this. For a subset of six soils, the reaction kinetics has been studied separately by extracting the samples for 4, 24, 48, 100, and 360 h.

The suspensions were shaken very gently to avoid abrasion that could change the amount of extracted PO_4, if new surface area would be created. A reciprocal shaker with a mild motion (~30 cycles/min) was used for the gentle mixing of the soil suspensions. The final reaction time was fixed at 10 or 15 days (~240 or 360 h), based on the above-mentioned study of the kinetics of the phosphate desorption. After equilibration, the soil suspensions were centrifuged to separate supernatant and solid. The sampled supernatant was carefully acidified to pH 2.0 by pipetting a calibrated volume of 1 M HCl and additionally diluted with 0.01 M HCl if necessary. The acidified (diluted) supernatant was analyzed spectrophotometrically for orthophosphate applying a molybdenum-blue method using a Segmented Flow Analysis (SFA) device.

For a number of samples, the pH values of the soil suspensions have been checked after completion of the experiment to ensure that the conditions of the soil suspensions were not changing throughout the experiment. Since Ca, Mg, and Si potentially may interfere in the phosphate adsorption process, these concentrations have also been measured in the extracts of a limited number of samples using ICP-AES.

2.4. Surface complexation modeling

Surface complexation models are based on thermodynamic principles that do not require an exclusive molecular picture. It implies that a good model description can be found using surface species that have no link to the microscopic state. If the challenge is to use realistic surface species, as observed with spectroscopic methods, many of these SCM cannot be used, because the framework to define such realistic species is not suitable enough. For instance, in the generalized two layer (GTL) model (Dzombak and Morel, 1990), the interface is simplified to a surface plane and a diffuse double layer (DDL) that neutralizes the surface charge. This conceptual structure does not allow distinguishing inner- and outer-sphere complexation. The same can be said with respect to the constant capacitance (CC) model in which the double layer is simplified to an electrical condenser. More realistic is the use of a DDL with at least one Stern layer (Stern, 1924), resulting in a basic or an extended Stern layer model (Westall and Hohl, 1980). Many SCM's use a generic reactive site, SOH^0, that can be traced back to the work of Parks and

De Bruyn (1962). For Fe and Al (hydr)oxides, the generic site (SOH^0) is actually a combination of two surface groups ($SOH^{-1/2}$ and $SOH_2^{+1/2}$) as pointed out by Hingston et al. (1968). The use of a generic SOH^0 site will lead by definition to an incorrect formulation of ion complexation reactions such as mono-, bi-, and tetra-dentate complex formation (Hiemstra and Van Riemsdijk, 1999).

A specific problem in the use of realistic surface species has been the reduction of the charge of surface complexes to a single point charge. This simplification strongly affects the computation of the electrostatic interaction energy and ignores that a surface species experiences the gradient of the electrostatic potential in the compact part of the double layer. The charge distribution (CD) concept can be used to account for this phenomenon (Hiemstra and Van Riemsdijk, 1996). In this model approach, part of the formal charge of an inner-sphere complex is attributed to the surface and the remaining part is present at some distance from the surface. It has been shown that the interfacial charge distribution is strongly linked to the molecular structure of inner-sphere surface complexes (Hiemstra et al., 2004; Hiemstra and Van Riemsdijk, 2006, 2007; Rietra et al., 1999).

In the present evaluation of the reactive surface area, the CD model (Hiemstra and Van Riemsdijk, 1996) will be used. As pointed out, it has the advantage that one may use realistic surface species as observed with spectroscopy and the model is able to describe successfully ion interactions in multi-component systems as recently demonstrated in the work of Stachowicz et al. (2008). Another advantage is that the model has been extensively parameterized in a consistent manner for a large number of ions that may bind to a high-surface area goethite. The parameter set covers at present the major cations (Na^+, K^+, Ca^{2+}, Mg^{2+}, Al^{3+}, Fe^{2+}), major anions (Cl^-, HCO_3^-, NO_3^-, SO_4^{2-}), and neutral species ($H_4SiO_4^0$) that are present in the natural aqueous phase and may interact with additionally present ions such as phosphate and many others minors.

The primary surface charge of goethite can be described by proton binding to two types of surface groups, which are singly ($\equiv FeOH^{-1/2}$) or triply ($\equiv Fe_3O^{-1/2}$) coordinated to Fe in the solid (Table 2). The effective site density is set at, respectively, $N_s = 3.45\ nm^{-2}$ and $N_s = 2.7\ nm^{-2}$ (Hiemstra et al., 1996). The charged surface groups may interact with electrolyte ions forming ion pairs and in addition, they may form inner-sphere complexes with other ions. Both types of surface complexes are located differently in the electrostatic double layer (EDL).

As mentioned, the simplest but realistic EDL approach comprises a diffuse double layer (DDL) that is separated from the surface by a Stern layer. At the surface, the primary protons reside, and the charge of electrolyte ion pairs can be attributed to the other electrostatic plane (1-plane). This plane represents the minimum distance of approach of electrolyte ions (ion pairs). According to the CD model (Hiemstra and Van Riemsdijk, 1996), the charge of the inner-sphere complexes can be distributed between the planes at either side of the Stern layer. Recently, it has been suggested for goethite that the head end of the DDL is separated from the minimum distance of approach of indifferent electrolyte ions by a second Stern layer (Hiemstra and Van Riemsdijk, 2006; Rahnemaie et al., 2006). The physical explanation is the increasing ordering of water molecules in one or several layers near the surface, which only allows a stepwise penetration of electrolyte ions into the compact part of the EDL (Hiemstra and Van Riemsdijk, 2006). The resulting double layer representation has three planes (0-, 1-, 2-plane) and two Stern layers with a capacitance of $C_1 = 0.93\ F/m^2$ and $C_2 = 0.74\ F/m^2$ (Table 2). The model can be called an Extended Stern layer model (Westall and Hohl, 1980) and is very similar to the recently adapted Triple Layer (TL) model (Sverjensky, 2005).

For goethite, the pH dependent adsorption behavior of phosphate has been studied extensively (Rahnemaie et al., 2007b). The goethite-phosphate interaction can be described using two surface species (Table 2). In-situ FTIR spectroscopy (Tejedor-Tejedor and Anderson, 1990) suggests the dominant presence of a bidentate double corner complex $\equiv (FeO)_2PO_2$. According to Rahnemaie et al. (2007b), a protonated monodentate complex ($\equiv FeO\text{-}PO_2OH$) may additionally form at high loading and low pH. The monodentate species explains the CD value that emerges from the data analysis of the phosphate adsorption (Rahnemaie et al., 2007b). The reactions can be expressed in terms of reference components, leading to:

$$2 \equiv FeOH^{-1/2} + PO_4^{3-}(aq) + 2H^+(aq) \Longleftrightarrow \equiv (FeO)_2^{-1+\Delta z_0}PO_2^{\Delta z_1} + 2H_2O(l); K_{(FeO)_2PO_2} \quad (1a)$$

and

$$1 \equiv FeOH^{-1/2} + PO_4^{3-}(aq) + 2H^+(aq) \Longleftrightarrow \equiv FeO^{-1/2+\Delta z_0}PO_2OH^{\Delta z_1} + 1H_2O(l); K_{FeOPO_2OH} \quad (1b)$$

The charge distribution of these surface complexes (Δz_0, Δz_1) has been derived from the geometry of the surface complexes that has been obtained by molecular orbital calculations (MO) using Density Functional Theory (DFT).

The phosphate–bicarbonate interaction has been studied for goethite in the concentration range 0–0.5 M $(H)CO_3$ (Rahnemaie et al., 2007a). The main carbonate surface species is a bidentate double corner complex (Bargar et al., 2005; Hiemstra et al., 2004). Its formation can be written as:

$$2 \equiv FeOH^{-1/2} + CO_3^{2-}(aq) + 2H^+(aq) \Longleftrightarrow \equiv (FeO)_2^{-1+\Delta z_0}CO^{\Delta z_1} + 2H_2O(l); K_{(FeO)_2CO} \quad (2a)$$

For this complex, the charge distribution has also been derived from the MO–DFT optimized geometry (Rahnemaie et al., 2007a).

CD modeling (Rahnemaie et al., 2007a) suggests that the carbonate complex (Eq. (2a)) may interact at a high electrolyte concentration with a Na^+ ion leading to:

$$2 \equiv FeOH^{-1/2} + CO_3^{2-}(aq) + 2H^+(aq) + Na^+(aq) \Longleftrightarrow \equiv (FeO)_2^{-1+\Delta z_0}CO\text{–}Na^{\Delta z_1} + 2H_2O(l); K_{(FeO)_2CO\text{–}Na} \quad (2b)$$

In addition, the protonated surface groups may interact with CO_3^{2-} forming outer-sphere complexes (Bargar et al., 2005), i.e. $\equiv FeOH_2^{+1/2} - CO_3^{2-}$ and $\equiv Fe_3OH^{+1/2} - CO_3^{2-}$ (Table 2).

Table 2
Tableau defining the formation reactions of surface species in the CD model using the extended stern layer option with $C_1 = 0.93$ and $C_2 = 0.75$ F/m^2.

Surface species	$\equiv FeOH^{-1/2}$	$\equiv Fe_3O^{-1/2}$	$\equiv HNOM^{-1}$	Δz_0	Δz_1	Δz_2	H^+	Na^+	K^+	Ca^{2+}	Mg^{2+}	Cl^-	PO_4^{3-}	CO_3^{2-}	log K
$\equiv FeOH^{-1/2}$	1	0	0	0	0	0	0	0	0	0	0	0	0	0	0
$\equiv FeOH_2^{+1/2}$	1	0	0	+1	0	0	1	0	0	0	0	0	0	0	9.0
$\equiv FeOH^{-1/2}...Na^+$	1	0	0	0	+1	0	0	1	0	0	0	0	0	0	-0.60 ± 0.03
$\equiv FeOH^{-1/2}...K^+$	1	0	0	0	+1	0	0	0	1	0	0	0	0	0	-1.61 ± 0.13
$\equiv FeOH_2^{+1/2}...Cl^-$	1	0	0	+1	−1	0	1	0	0	0	0	1	0	0	8.55 ± 0.03
$\equiv Fe_3O^{-1/2}$	0	1	0	0	0	0	0	0	0	0	0	0	0	0	0
$\equiv Fe_3OH^{+1/2}$	0	1	0	+1	0	0	1	0	0	0	0	0	0	0	9.0
$\equiv Fe_3O^{-1/2}...Na^+$	0	1	0	0	+1	0	0	1	0	0	0	0	0	0	-0.60 ± 0.03
$\equiv Fe_3O^{-1/2}...K^+$	0	1	0	0	+1	0	0	0	1	0	0	0	0	0	-1.61 ± 0.13
$\equiv Fe_3OH^{+1/2}...Cl^-$	0	1	0	+1	−1	0	1	0	0	0	0	1	0	0	8.55 ± 0.03
$\equiv (FeO)_2PO_2$	2	0	0	0.46	−1.46	0	2	0	0	0	0	0	1	0	29.72 ± 0.01
$\equiv FeOPO_2OH$	1	0	0	0.28	−1.28	0	2	0	0	0	0	0	1	0	27.63 ± 0.01
$\equiv (FeO)_2CO$	2	0	0	0.62	−0.62	0	2	0	0	0	0	0	0	1	22.01 ± 0.02
$\equiv (FeO)_2CO...Na^+$	2	0	0	0.62	0.38	0	2	1	0	0	0	0	0	1	22.03 ± 0.05
$\equiv FeOH_2^{+1/2}...CO_3^{2-}$	1	0	0	+1	−2	0	1	0	0	0	0	0	0	1	10.22 ± 0.20
$\equiv Fe_3OH^{+1/2}...CO_3^{2-}$	0	1	0	+1	−2	0	1	0	0	0	0	0	0	1	10.22 ± 0.20
$\equiv FeOH^{-1/2}Ca^{2+}$	1	0	0	0.31	1.69	0	0	0	0	1	0	0	0	0	3.23 ± 0.05
$\equiv FeOH^{-1/2}CaOH^+$	1	0	0	0.31	0.69	0	−1	0	0	1	0	0	0	0	-6.42 ± 0.08
$\equiv FeOH^{-1/2}...Ca^{2+}$	1	0	0	0	+2	0	0	0	0	1	0	0	0	0	1.8 ± 0.95
$\equiv Fe_3O^{-1/2}...Ca^{2+}$	0	1	0	0	+2	0	0	0	0	1	0	0	0	0	1.8 ± 0.95
$\equiv (FeOH)_2{}^{-1}Mg^{2+}$	2	0	0	0.72	1.28	0	0	0	0	0	1	0	0	0	4.52 ± 0.02
$\equiv (FeOH)_2{}^{-1}MgOH^+$	2	0	0	0.72	0.28	0	−1	0	0	0	1	0	0	0	-6.78 ± 0.07
$\equiv FeNOM^{0-1-0.5*}$	1	0	1	1.5	−1	−0.5	0	0	0	0	0	0	0	0	0
$CaCO_3$ (soil)[#]	0	0	0	0	0	0	0	0	0	1	0	0	0	1	log $K_{so} = -8.4$

[*] Not used for the speciation calculations in the $NaHCO_3$ extracts, because of the assumed absence of interaction of NOM. The site density N_{HNOM} (Table 1) of the hypothetical species $\equiv$ FeNOM has been calculated using Eq. (1) in part II (Hiemstra et al., 2010), interpreting the PO_4 concentration in 0.01 M $CaCl_2$ solution. The charge at the 0-, 1-, and 2-plane after formation of FeNOM is, respectively, 0, −1, and −0.5 v.u. which is created by redistribution of the total reference charge of −1.5 v.u., see text in part II (Hiemstra et al., 2010).
[#] For the Bakers Hill soil, log $K_{so} = -7.3$ has been used.

The adsorption of phosphate and also carbonate may be influenced by the presence of Ca^{2+} (Rietra et al., 2001; Stachowicz et al., 2008). In a 0.5 M $NaHCO_3$ solution, the Ca^{2+} activity is rather limited by the formation of solid $CaCO_3$ (s). In soil, part of the Ca^{2+} ions are initially adsorbed by organic matter and clay and will be released by ion exchange when $NaHCO_3$ is added in a high concentration. CD modeling suggests that calcium ions may bind as inner- and outer-sphere complexes at the goethite surface (Rietra et al., 2001; Stachowicz et al., 2008). For Mg^{2+}, only the formation of a bidentate inner-sphere surface complex can be resolved (Stachowicz et al., 2008). For the divalent cations, the model has been calibrated on proton titration data (Rahnemaie et al., 2006) in the presence of Ca^{2+} and Mg^{2+} and has been tested on a collection of Ca^{2+} and Mg^{2+} adsorption data given in Stachowicz et al. (2008). The present parameter set for Ca^{2+} and Mg^{2+} slightly differs from the set of Stachowicz et al. (2008) to be consistent with the other parameters that refer to a goethite with a slightly lower PZC (Rahnemaie et al., 2007a,b). The parameters are given in Table 2.

The surface complexation modeling was done with the ECOSAT software (Keizer and Van Riemsdijk, 1998) in combination with FIT (Kinniburgh, 1993). The aqueous speciation reactions used are given in the Appendix.

3. RESULTS AND DISCUSSION

3.1. Desorption kinetics

Barrow and Shaw (1976b) studied extensively a number of factors that can affect the phosphate extraction by bicarbonate, such as the time dependency of desorption. Initially, the phosphate desorption rate was quite high, slowed down in some hours, but the desorption starts to reverse at prolonged extraction times (~10–200 h). This effect was stronger at high solid–solution ratios. This remarkable behavior may be due to the pretreatment of the samples. These samples originated from a virgin soil but were loaded artificially with phosphate in the lab. Although these samples were incubated for two years, the artificial P-loading may have led to a relatively high saturation of particularly the external surfaces leaving the core of the (micro) aggregates relatively unaffected. At prolonged times of extraction, the soil particles may progressively disintegrate, leading to the exposure of pristine surfaces, previously not sufficiently loaded with phosphate. The gradually uncovered surfaces may adsorb some phosphate that has been released in the extraction from the higher loaded parts. The increased exposure of a soil due to abrasion is supported by an additional observation (Barrow and Shaw, 1975) showing that vigorous shaking of these preloaded soil samples led to more phosphate binding to probably previously internal surface area.

In the present work, the soil samples have been loaded with phosphate in nature during long-term agricultural practices. We expect that this will lead to a more even distribution over external and internal surfaces. Six samples of our collection were selected randomly to study the desorption kinetics. The time dependency of the bicarbonate extraction was studied for different solid–solution ratios. The effect of varying the SSR is shown in Fig. 1a for soil sample S2 in detail, and in Fig. 1b, it is shown for all six soils that were selected to study the kinetics.

Fig. 1a shows an instant release of phosphate when the bicarbonate solution is added. It is followed by an additional increase of the concentration to an apparent equilibrium state that is approached at longer time scales. In Fig. 1b, the desorption kinetics are shown for six samples using a SSR of 1/5 and 1/100 kg/L. In contrast to the results shown by Barrow and Shaw (1976b), no re-adsorption of phosphate and corresponding decrease of the phosphate concentration is observed at prolonged periods of shaking. This may point to more homogeneity in the P distribution over the soil matrix and less abrasion of the soil material. Based on the measurements, further experiments were done using for most samples 360 h (15 days) of equilibration. Some samples were equilibrated for 10 days.

3.2. Mechanism

A remarkable characteristic of the desorption process is the fast initial release that depends on the SSR. This fraction of phosphate can be interpreted as bound at external surfaces of soil oxides. The further release of phosphate may come from interior parts of the metal oxide aggregates. Slow release of phosphate is generally observed in soils that are extracted with a low or very low solid–solution ratio, forcing phosphate to diffuse out of the porous matrix to meet ultimately an equilibrium criterion at a low PO_4 concentration. In case of extraction of soils with a low solid–solution ratio using water or a simple electrolyte solution such as 0.01 M $CaCl_2$, the phosphate desorption is usually very slow (Koopmans et al., 2004). If explained in terms of diffusion, it is due to the small gradient of the phosphate concentration within the aggregates. As described later, embedding of oxide particles in a condensed matrix of natural organic matter molecules may also contribute to this kinetic behavior. A low SSR will ultimately lead to a large release of phosphate, but the rate of desorption is quickly reduced because a little decrease of the loading already leads to a strong decrease of the equilibrium concentration. This follows from the high-affinity character of the phosphate adsorption isotherm. The low phosphate concentrations created in the interior of the aggregates will make the diffusion gradient and corresponding rate (very) low.

To improve the efficiency of desorption, one may add a competitive ion. In our case, bicarbonate ions are used. If added in a high concentration, these ions will quickly diffuse into the porous matrix and desorb phosphate locally, resulting in a relatively high PO_4 concentration in the interior and a corresponding relatively large concentration gradient and rate of diffusion. Moreover, the competition between carbonate and phosphate will change the shape of the adsorption isotherm. It will get a less high-affinity character, which will maintain for a longer time a high gradient and corresponding rate of diffusion. The presence of the competitor in the interior may also lead to redistribution of PO_4 inside the porous micro-aggregates that are internally not in equilibrium state. This process may also

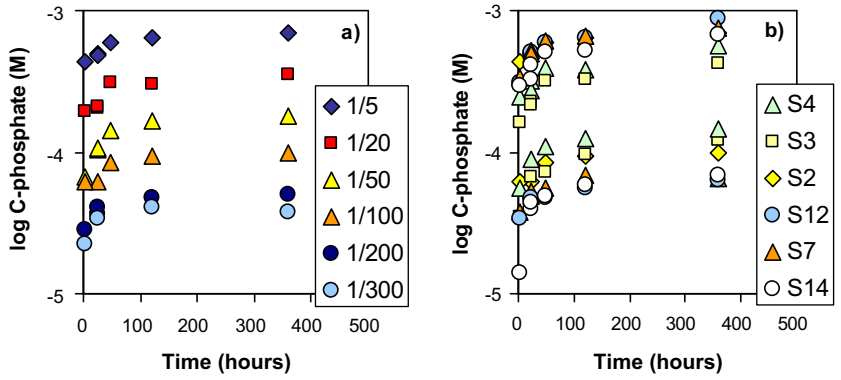

Fig. 1. (a) Time dependency of the release of phosphate from a soil sample (S2) extracted with 0.5 M bicarbonate (pH = 8.5) at various solid–solution ratios (SSR) and (b) the desorption kinetics for a selected set of samples for SSR = 1/5 (highest set of concentrations) and 1/100 kg/L (lowest set of concentrations).

contribute to the observed decrease of the phosphate concentration in $NaHCO_3$ extracts of a rapidly P-loaded soil sample at prolonged times of equilibration as used by Barrow and Shaw (1976b).

A kinetic process with two-steps has also been found in some studies of the adsorption of phosphate by synthetic mineral oxides (Luengo et al., 2006; Torrent et al., 1990). The data presented by Strauss et al. (1997) revealed that many iron oxides have a fast initial adsorption process, followed by a slower process that may last for several days or even weeks. There is still some controversy about the mechanisms involved in the slow process, but Torrent et al. (1992) suggested that this slow step is a slow diffusion of phosphate to the surface of pores located between domains of contiguous crystals or between aggregated particles. The ATR-IR results found by Luengo et al. (2006) are compatible with this mechanism for the slow adsorption process, which allow them to conclude that the surface complexes formed after the first minutes of reaction migrate rather slowly into the pores of the mineral surface without changing appreciably their identity.

3.3. Phosphate loading and buffering

Fig. 2 illustrates the change of the phosphate concentration (c) in the $NaHCO_3$ solution at near-equilibrium conditions upon varying the SSR for five representative soils. The highest phosphate concentrations are found at the highest SSR. These concentrations differ by a factor 20 for the samples in our data set. It illustrates that the chosen soils will clearly differ in phosphate loading per unit surface area. As will be shown later, the PO_4 loading is between about 1–3 μmol/m^2 in our soils.

As follows from the graph, the concentrations decrease when the solid–solution ratio decreases. If the solid would not release any phosphate, a linear curve is expected because then only dilution of the free soil solution takes place. In the log–log plot of Fig. 2, the slope of a linear dilution curve is 1, equal to the slope of the dotted line. The trend in the data deviates from such a linear curve, most strongly at the highest solid–solution ratios. This is due to a non-linear release of PO_4 from the soil matrix at dilution of the

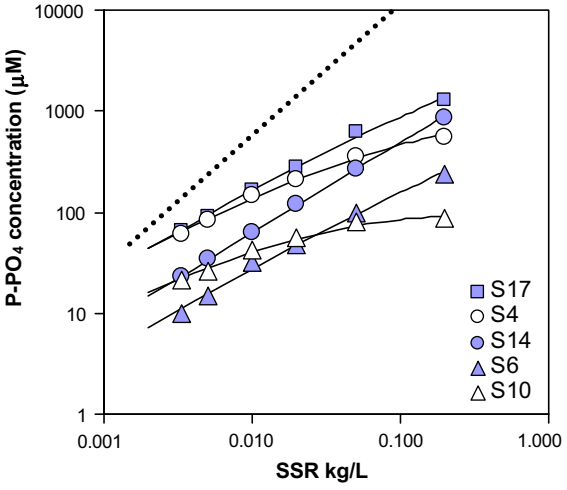

Fig. 2. The change of the phosphate concentration as a function of the solid–solution ratio in 0.5 M $NaHCO_3$ at pH 8.5 for soils that differ in non-linear phosphate buffering because of differences in reactive surface area. The full lines are fitted to the CD model using Table 2. Saturation of the solution with calcite was assumed. The dotted line represents a linear dilution curve.

sample (lower SSR). It may be expected that soils with the lowest variation in the phosphate concentration, i.e. the highest buffering, will have a relatively high reactive surface area. This is discussed next.

3.4. Solid–solution distribution

For a given adsorption behavior, the deviation from the linear dilution curve is related to the amount of effective reactive surface area A (m^2/kg soil) available in the sample. In the probe–ion extraction, the total amount of phosphate per unit mass that can be bound reversibly (R_{ev} in mole per kg soil) is a constant, given by the field conditions in the soil when sampled. The total amount of reversible phosphate is distributed over solid and solution during equilibration, which leads to the following mass balance:

$$R_{ev} = A\Gamma + \rho^{-1}c \qquad (3)$$

in which Γ is the phosphate adsorption per unit effective reactive surface area (mol/m^2), and ρ is the solid–solution ratio SSR (kg/L). When the SSR (ρ) is lowered, the experimental phosphate concentration (c) in solution will decrease (Fig. 2). This will lead to a lower phosphate adsorption (Γ). If the adsorption isotherm (i.e. the relation $\Gamma \leftrightarrow c$), expressed per unit surface area is known, we may calculate the effective reactive surface area A (m^2/kg soil) from:

$$A = -\frac{\Delta(\rho_i^{-1} c_i)}{\Delta \Gamma_i} \tag{4}$$

in which Δ indicates the change of the indicated parameter values with index $i = 1$ and 2. Once A is calculated, we may also find the total amount of phosphate that is reversibly adsorbed by the sample (R_{ev}). Interestingly, the total amount of reversibly adsorbed phosphate (R_{ev}) can be found even though only a small fraction of the total amount is extracted and redistributed over the solid and solution phase in the equilibrium state. To find R_{ev}, a total extraction is not at all required. Only correct numbers for A and R_{ev} will be found if the actual phosphate adsorption isotherm of the material (i.e. the equilibrium relation $\Gamma \leftrightarrow c$) is sufficiently accurately approached for the conditions applied. In our approach, Γ is calculated with the CD model for every experimental value of c. In principle, a minimum of two concentrations is sufficient to calculate the effective reactive surface area (Eq. (4)), but in the present approach, we have used six different solid–solution ratios (ρ). The reason is that the fitted parameters are sensitive to small variations in the experimental concentration.

Before applying the probe ion method to our samples, we tested the ability of the CD model to describe the competitive phosphate adsorption behavior for a soil at pH 8.5 as a function of the $NaHCO_3$ solution concentration. Such experimental data are available in literature for an Australian soil from Bakers Hill (Barrow and Shaw, 1976b) as given in Fig. 3. The pristine soil has been incubated in advance with phosphate and aged at 70 °C. The experiments have been carried out at different solid–solution ratios. The ionic strength has been kept constant at 1 M by adding additional NaCl. Unfortunately, the extraction time has been only 16 h.

The data show a strong influence of the HCO_3^- concentration, which is most significant in the concentration range below about 0.5 M. However, the highest PO_4 desorption (per unit mass of soil material) is for the lowest solid–solution ratio, where the low concentration nevertheless represents a large amount of phosphate because of the relatively large solution volume per unit mass. As shown by Barrow and Shaw (Barrow and Shaw, 1976b), the maximum desorption is about 30% of the initially added P when extracted at a SSR of 1:300. In case of a SSR of 1:6, the maximum desorption is only about 15% in 0.5 M $NaHCO_3$. In other words, most of the phosphate (>70 to >85%) remains bound.

3.5. Modeling

The adsorption of carbonate by the soil of Bakers Hill (Fig. 3) has been modeled with the CD model using the parameters of Table 2. The effective reactive surface area (A m^2/kg soil) was the only adjustable parameter in Eq. (3) in combination with the amount of reversibly bound phosphate (R_{ev} mol/kg). It may be assumed that the Ca^{2+} activity in the (H)CO_3 solutions (pH = 8.5) is controlled by a $CaCO_3$ phase. The lowest calcium carbonate solubility is for calcite (log $K_{so} = -8.4$). However, well-crystallized calcite may not be instantaneously formed at precipitation. A more soluble meta-stable $CaCO_3 .x\ H_2O$ phase may form first. Amorphous calcium carbonate as well as mono- ($x = 1$) and hexa-hydrated ($x = 6$) calcium carbonate are more soluble. The reported solubility products are, respectively, log $K_{so} = -6.4$, -7.2, and -7.6 (Brecevic and Kralj, 2007). To asses the solubility product that may be appropriate for the calcium carbonate freshly formed in the $NaHCO_3$ extraction solution of the Bakers Hill soil (Fig. 3), we have fitted simultaneously also the calcium carbonate solubility, leading to log $K_{so} = -7.4 \pm 0.1$. This number is close to the solubility of $CaCO_3{\cdot}H_2O$ (s). This mineral can be found in dynamic lake sediments and is relatively stable if ions such as Mg^{2+} are present (Brecevic and Kralj, 2007). The effective reactive surface area of the Baker Hill soil that has been fitted equals $A = 5.5 \pm 0.1$ m^2/g soil. The quality of the fit (Fig. 3) shows that the CD model is able to describe the competition of phosphate and carbonate in a soil in $NaHCO_3$/NaCl solutions at pH 8.5. We note that the further modeling indicated that the influence of Ca^{2+} is limited to those systems of Fig. 3 that have the lowest (H)CO_3 concentrations but correspondingly the highest Ca^{2+} activities. The Ca^{2+} ions, when adsorbed, promote the adsorption of PO_4 (Rietra et al., 2001) and suppress the phosphate concentration.

As mentioned above, the fitted surface area should be considered as an effective reactive surface area. The behavior of the soil oxide fraction is effectively represented by the behavior of the goethite mineral for which the model has been calibrated. The effective surface area (A) of the soil (m^2/g soil) can be transformed into an effective specific sur-

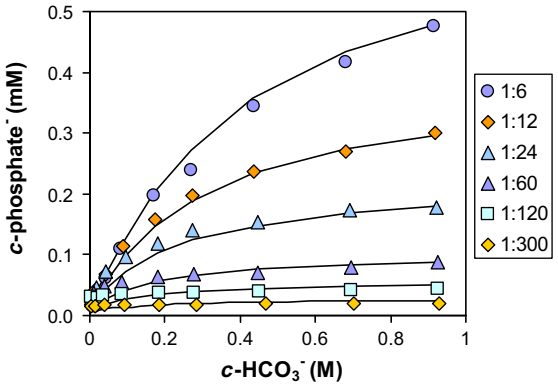

Fig. 3. Effect of bicarbonate concentration and soil–solution ratio on the phosphate concentration equilibrated for 16 h with soil of Bakers Hill (Barrow and Shaw, 1976a,b). The lines show the simulated phosphate concentrations in the extraction solutions (a mixture of NaCl and $NaHCO_3$, $I = 1$ M) using the CD model and the parameters of Table 2. Saturation of the solution with $CaCO_3{\cdot}H_2O$ (s) was assumed (see text).

face area (SSA) for the metal oxide fraction of the soil (m^2/g oxide). The free Fe and Al content, extractable with the method of Coffin (Coffin, 1963) is 2 mg Fe/g and 1.8 mg Al/g soil (Barrow and Shaw, 1975), equivalent with approximately 8 mg oxide/g soil. This results in a SSA of about 700 m^2/g sesquioxides. It suggests that the reactive metal oxide fraction in this soil consists of very small oxide particles with a SSA, which is typically for ferrihydrite (Hiemstra and Van Riemsdijk, 2009).

The amount of reversibly bound phosphate equals $R_{ev} = 11.1 \pm 0.1$ mmol/kg, when fitted simultaneously with A. This number is slightly lower than the amount of PO_4 added to the pristine soil, i.e. 400 μgP/g soil or ~13 mmol/kg. It suggests that more than ¾ of the added PO_4 can be recovered. A lower recovery might be due to non-equilibrium or some of the phosphate has been transformed into an insoluble mineral fraction.

3.6. Data Copernicus soil series

For some of our own soil samples, we have measured the Ca^{2+} concentration in the (bi)carbonate extract after equilibration for 10–15 days, revealing an apparent $CaCO_3$ solubility product of $\log K_{so} = -8.5 \pm 0.3$. Within the error, this number is equal to the solubility product of calcite. It deviates from the above apparent log K value for freshly precipitated $CaCO_3$ which may be due to difference in aging (16 h versus 10–15 days). In the further calculations, we have used for our soils the solubility of calcite, but we note that the effect of Ca^{2+} is minor for soils in 0.5 M $NaHCO_3$.

In the extracts, the Si concentrations were in general between ~0.2–2 mg Si/L and about 2–10 times lower than the phosphate concentrations. Based on modeling (Hiemstra et al., 2007), it is expected that in our soils the relatively low Si level will have no important influence on the phosphate loading.

The total amount of reversibly bound phosphate (R_{ev}) and the effective surface area (A) have been fitted for each sample. The quality of the fit ($n = 6$ data points) was usually high ($R^2 > 0.98$–0.99). As illustration, the model descriptions are shown as lines for the selected soils in Fig. 2. We have evaluated our data using for the phosphate concentration the linear and the logarithmic scale. The fitted average values of A and R_{ev} are presented in Table 1. The given deviation (±) is related to the chosen scaling of the concentration. For our set of soils, the effective reactive surface area varies by a factor of about 10 and is between about 3 and 30 m^2/g soil. The total amount of reversibly bound phosphate R_{ev} also varied strongly amongst the samples. When expressed per m^2 oxide surface, the phosphate loading in the soils differs by about a factor 2–3, covering the range $R_{ev}/A = \Gamma \approx 1$–$3$ μmol/m^2. Considering the high-affinity character of the phosphate adsorption isotherms ($\Gamma \leftrightarrow c$) in a $CaCl_2$ solution (Barrow et al., 1980), this variation in Γ is remarkably high compared to the relatively small variation in the equilibrium concentration (c) of phosphate in 0.01 M $CaCl_2$ ($c \approx 1$–30 μM) and pH (4–7). The larger variation in phosphate loading is due to the interaction with NOM, as is further discussed in more detail in Part II of this series (Hiemstra et al., 2010).

3.7. Reversibly adsorbed phosphate

The reversibly bound phosphate content R_{ev} (mmol/kg) can be compared with the phosphate fraction that is found by other approaches such as an extraction with ammonium oxalate. This comparison is shown in Fig. 4. The data in the lower range are often slightly above the 1:1 relationship (dotted line), i.e. more PO_4 is extracted with oxalate. If an enhanced extraction of PO_4 with oxalate is realistic for these soils, it may point to a contribution of phosphate from another source. Oxalate dissolves simultaneously Fe and Al ions and this dissolution may release some additional phosphate that is otherwise present in the soil matrix as for instance occluded phosphate (Walker and Syers, 1976) or as phosphate being part of a mineral phase or a co-precipitate. The latter has been proposed for highly fertilized soils (Vanderzee and Vanriemsdijk, 1988), marine sediments (Hyacinthe and Van Cappellen, 2004), and lake and ground waters (Griffioen, 2006; Lienemann et al., 1999; Wolthoorn et al., 2004).

At high phosphate contents, the predicted total amount of reversibly bound PO_4 (R_{ev}) is in some cases significantly larger than the amount found in the oxalate extract, in particular if the data are evaluated on a linear concentration scale for phosphate in the $NaHCO_3$ experiments. For a given P-loading per unit surface area (μmol/m^2), a slightly higher amount of calculated PO_4 (R_{ev}) will also imply the calculation of a slightly too high-surface area. It is possible that the assumed phosphate adsorption behavior (model) is not entirely reflecting the actual adsorption properties of the natural oxide fraction and this can be due to many factors, including an incomplete removal of adsorbed NOM. This problem cannot be solved yet but needs future attention.

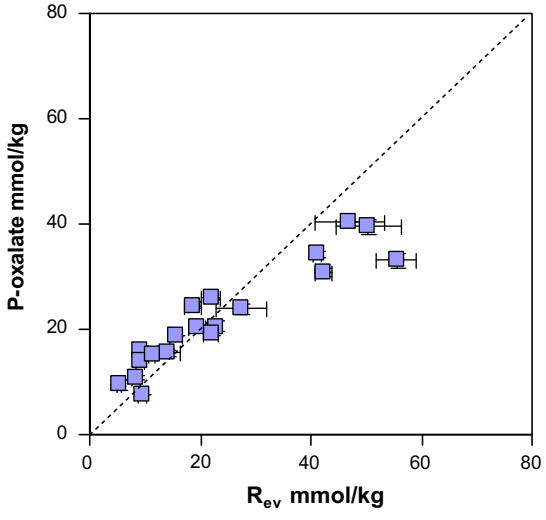

Fig. 4. The amount of phosphate extracted with ammonium oxalate (P_{ox}) in relation to the calculated amount of reversibly adsorbed phosphate (R_{ev}). The dotted line represents the 1:1 relationship. In case of high phosphate contents, a higher amount of reversibly bound P is calculated than found with oxalate.

3.8. Surface area and specific surface area

The effective reactive surface areas calculated for our soils are only weakly correlated ($R^2 = 0.45$ for $n = 19$) with the oxalate extractable fraction of Fe and Al (Fig. 5, full line). A similar result is found when using the DCB extractable Fe and Al fraction (not shown). A low correlation is expected if variation exists in the size of the oxide particles and its corresponding effective specific surface area (SSA). The mean effective SSA is represented by the slope of the line in Fig. 5. Between the samples, the effective SSA differs by about a factor 5.

As mentioned in the Introduction, the surface area of soil oxides is often calculated based on a Fe and Al (hydr) oxide extraction and an assumed SSA. If the surface areas are scaled to the amount of Fe and Al (hydr) oxides extractable with oxalate, the average SSA is about 1000 ± 790 m^2/g. If scaled on the amount of (hydr) oxides extractable with DCB, the average SSA equals 720 ± 540 m^2/g. The high value of the SSA suggests the presence of very small (hydr)oxide particles and the very large variation indicates that no single SSA can be used for the natural oxide fraction to asses the reactive surface area based on Fe and Al extraction methods.

The above-calculated SSA is based on an assumed molar mass of $M = 89$ g/mol Fe (goethite) and $M = 78$ g/mol Al (gibbsite). However, it has been shown very recently (Hiemstra and Van Riemsdijk, 2009) that nanoparticles have an enhanced molar mass. This effect is about 15% for nanoparticles of this small size and corresponding large SSA. Therefore, the average SSA will actually be slightly smaller, i.e. about $\sim 630 \pm 470$ m^2/g (DCB). The thus-scaled SSA values are shown on the y-axis of Fig. 6.

If expressed in an equivalent diameter (d) for non-porous spherical particles with a typical mass density ρ of 3.5 g/cm^3 (Hiemstra and Van Riemsdijk, 2009), the effective diameter varies between $d \sim 1$–10 nm when calculated with $d = 6/(\rho\ \mathrm{SSA})$. Most samples in our study have an effective particle size that is typical for synthetic ferrihydrites. For instance, the particle size of freshly prepared two-line ferrihydrite varies between about 1.5 and 3.0 nm (Murphy et al., 1976), while for 6-line ferrihydrite the numbers are about 5–7 nm (Janney et al., 2000). Some of our samples have a very high effective SSA and the corresponding effective particle size is extremely low (about 1 nm). This may be partly due to an overestimation of the P content (R_{ev}) and corresponding surface area (A), see discussion at Fig. 4. The use of goethite as representative mineral may also contribute to this. If the natural oxide particles have a higher site density and a higher phosphate adsorption density, a lower effective surface area and a larger effective particle size will be found. Nevertheless, the formation of extremely small particles can also not be excluded yet. Recently, an interesting observation was reported by Eusterhues et al. (2008) showing that synthetic ferrihydrite will form considerably smaller particles when prepared in the presence of organic matter.

In Fig. 6, the SSA derived by the probe ion method is given as function of the relative phosphate loading. For scaling of the x-axis in the figure, we used for phosphate the amount extractable with oxalate and for Fe and Al the amount extractable with DCB, i.e. scaling on experimental data. The dotted line represents the theoretical relationship assuming for phosphate, extractable with oxalate, a reversible binding of 2 μmol/m^2. The upper and lower lines in Fig. 6 are for, respectively, 1 and 3 μmol/m^2 of oxalate extractable phosphate. This chosen range of phosphate loadings (1–3 μmol/m^2) is representative for the range in

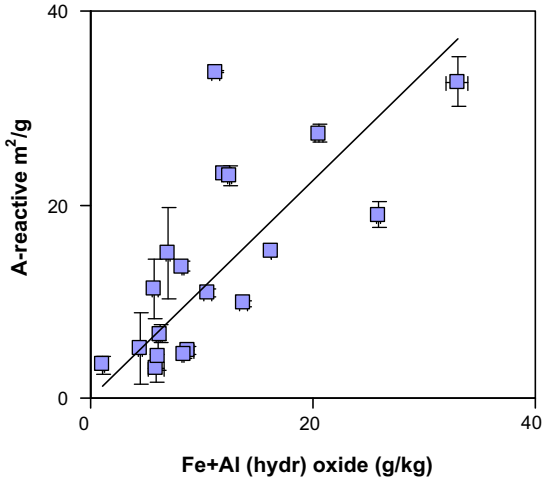

Fig. 5. The effective reactive surface area A as a function of the amount of Fe and Al (hydr)oxide (g/kg) extractable with ammonium oxalate, assuming a molar mass of 89 and 78 g/mol for, respectively, Fe and Al (hydr)oxide. The slope of the full line represents the mean specific surface area.

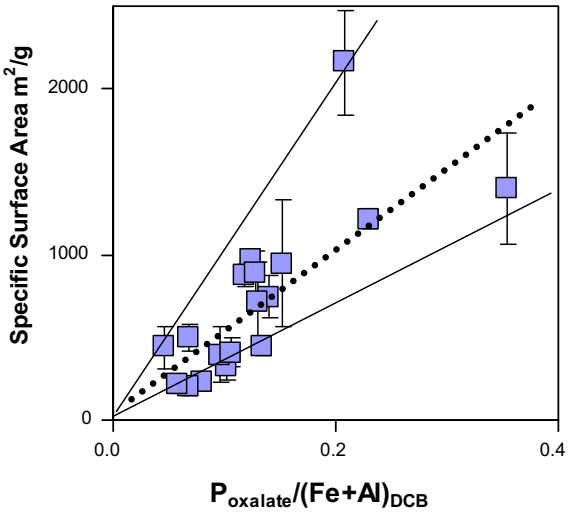

Fig. 6. The calculated effective specific surface area of natural metal oxide particles in agricultural top soils as function of the phosphate loading, defined as the ratio of oxalate extractable phosphate (mmol/kg) and amount of iron and aluminum extractable with DCB (mmol/kg). The dotted line refers to a phosphate loading of 2 μmol/m^2 at the surface of an oxide with a molar mass of 100 g/mole in the case that all phosphate is reversibly bound. The upper and lower full lines are for a loading of 1 and 3 μmol/m^2, respectively.

our soils found by modeling the equilibration of phosphate in 0.5 M $Na(H)CO_3$. As shown in Part II (Hiemstra et al., 2010), the phosphate loading of field samples is not only imposed by the average concentration of phosphate in the field, but is also strongly affected by the adsorption of organic matter and the presence of DOC in solution.

In principle, a small particle size will result in a higher solubility of the oxide particles, depending on the surface energy. Surface energy is related to a different ensemble of bonds in the interface compared to the bulk and therefore, it can be affected by ion adsorption (Weng et al., 2006). Recently, it has been suggested that the adsorption of oxyanions will lead to a reduction of the solubility of ferrihydrite particles (Fukushi and Sato, 2005). In particular, phosphate has a large effect in lowering the solubility of ferrihydrite making the particles relatively more stable. Increase of the loading will allow the presence of smaller particles at the same overall chemical stability. In other words, the presence of adsorbed phosphate can compensate an enhanced solubility due to a smaller particle size.

4. MINERAL–NOM ASSOCIATION

4.1. NOM-loading

The information about the effective surface area A of soils and specific surface area SSA of natural soil oxide particles can be very useful to sharpen our view on the nature of natural oxide fraction in relation to organic matter. In soils, natural organic matter is often associated with the finest mineral fractions (Eusterhues et al., 2003; Schulten and Leinweber, 2000). Radiocarbon dating shows that organic matter, bound by the mineral fraction, is relatively old (Eusterhues et al., 2003; Torn et al., 1997). This suggests that it is relatively stable which is in agreement with the work of Keil et al. (1994), and others (Torn et al., 1997; Wagai and Mayer, 2007).

In our study, a clear relationship is found between the effective reactive surface area A of the soils and the organic carbon content (Fig. 7a), with the exception of some soils with relatively very high organic carbon contents. For the selected set of soils with 5% organic carbon (OC) or less (dark data points, $n = 17$), linear regression results in $A\ (m^2/g) = 6.0\%\ OC$ ($R^2 = 0.92$). If only sandy soils (clay fraction $<8\%$) or sandy and loamy soils (clay fraction $\leqslant 12\%$) are considered, one finds in both cases $A\ (m^2/g) = 8.0\%\ OC$ ($R^2 = 0.97$ for $n = 10$). The average relationship is given as full line in Fig. 7a and the dotted line represents a four times higher carbon content per unit surface area. The observed correlation (full line) suggests the presence of an association of NOM with oxidic surfaces formed by Fe and Al (hydr)oxides and probably the edges of clay minerals. However, soils can also have quite some additional carbon (dotted line). This may be present at the planar faces of clay minerals, bound by intercalation (Eusterhues et al., 2003), but may also be present due to multilayer adsorption, leading to a higher carbon content per unit surface area in an oxide–NOM association. In addition, organic matter may be present as low-density organic matter (Wagai et al., 2008), which does not have a significant association with mineral particles and may be present in a coagulated/precipitated form.

For a further interpretation, we may express the amount of natural organic matter (NOM) in our samples per unit effective surface area. Using the average slope s of the above relationship ($s = 7.0 \pm 1$), the mean organic carbon content is $\sim 1.4 \pm 0.2$ mg OC/m^2. This is equivalent with $\sim 2.5 \pm 0.4$ mg NOM/m^2 in case of a carbon content of 58%. These results can be compared with literature data, but note that in literature the BET surface area has generally been used whereas our data refer to an oxidic surface area. The BET surface area should be measured after carbon removal, because organic matter may mask the actual mineral surface area (Kaiser and Guggenberger, 2003). For marine sediments, the carbon loading (Keil et al., 1994; Mayer, 1994) measured in this way, is in the order about 0.8 ± 0.1 mg OC/m^2 BET surface area. This loading is lower and this might be due to the different scale used for surface area, but it may also be related to a difference in the environmental conditions present in both systems (marine sediment versus agricultural top soils).

We may compare the apparent organic carbon loading with the adsorption maximum of natural organic acids at iron (hydr) oxide surfaces. The above OC loading ($\sim 1.4 \pm 0.2$ mg OC/m^2) is between the maximum loading of oxide surfaces with purified FA, ~ 0.6 mg OC/m^2 (Filius et al., 2000; Gu et al., 1996, 1994; Zhou et al., 2001), and HA, ~ 2.5 mg OC/m^2 (Antelo et al., 2007; Weng et al., 2007). This comparison shows that potentially a considerable part of the organic matter in the agricultural soils can be stored directly at the surface of the nano-oxide particles.

4.2. Structural model

To develop a structural picture of an oxide–NOM association (Fig. 7b), we may calculate the equivalent thickness of a hypothetical NOM layer at the particle surface based on the data of Fig. 7a. Assuming a mass density of 1250 kg NOM/m^3, the above NOM loading of 2.5 ± 0.4 mg NOM/m^2 has an equivalent thickness of $\sim 2.0 \pm 0.3$ nm. This number falls in the range of the size of natural organic acids like purified FA and HA molecules, which are about 1 and 3 nm, respectively, (Weng et al., 2007). In Fig. 7c, adsorbed HA is shown as an example. Only a small part of the NOM is present in the Stern layers. The compact part of the ES double layer is in total approximately 0.7 ± 0.2 nm (Hiemstra and Van Riemsdijk, 2006). The average equivalent thickness of NOM (2.0 ± 0.3 nm) is about half the average particle size of the natural oxides ($\sim 4.0 \pm 2.6$ nm) in the soils studied. In combination, the average equivalent particle size of humic acid coated oxide particle will be $\sim 8 \pm 3$ nm. Field flow fractionation (FFF) of the colloidal fraction (<0.2 μm) of a forest soil, shows nano-sized particles of a similar (hydrodynamic) diameter (Hassellov and Von der Kammer, 2008) as we have established.

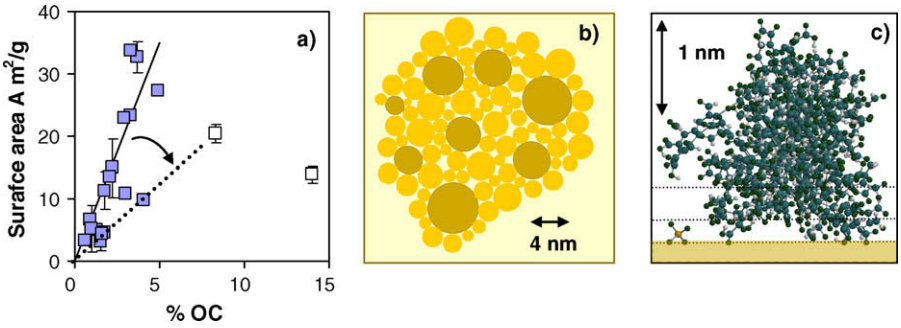

Fig. 7. (a) The effective reactive surface area as a function of the organic carbon content of the Copernicus soil series. At a relatively low% OC, the effective surface areas increase with the OC fraction (closed symbols). The full line refers to 1.4 mg OC/m^2, which is equivalent with NOM layer thickness of 2.0 nm. The dotted line refers to the presence of more carbon (5 mg OC/m^2). (b) A schematic 2D model for an organo-mineral association. The (micro) aggregate has oxide particles as darker spheres ($\sim 4.0 \pm 2.6$ nm) surrounded by a layer ($\sim 2.0 \pm 0.3$ nm) of attached organic matter molecules ($\sim 1.4 \pm 0.2$ mg OC/m^2) that have an average NOM volume fraction of about 80%. The aggregate has an average mass density of ~ 1.7 g/cm^3. The NOM molecules have a variable degree of chemical interaction with the mineral surface groups depending on factors like pH and phosphate loading. (c) NOM molecule ($M \sim 10{,}000$ Da) attached to a mineral surface in comparison to a phosphate ion (left side in 7c). The horizontal dotted lines represent the electrostatic Stern planes of the ES model. NOM and PO_4 dominantly interact via the ligand distribution in the inner Stern layer space.

The surface loading with carbon can be brought into further perspective by expressing the presence of both, organic matter and mineral particles, as a volume. In the calculation, the mass density of ferrihydrite (Fh) and NOM is set at, respectively, 3500 kg/m^3 (Hiemstra and Van Riemsdijk, 2009) and 1250 ± 150 kg/m^3. The calculated volume ratio NOM/Fh for oxide particles with an average specific surface area of ~ 630 m^2/g equals approximately 4.4 m^3 NOM/m^{3}Fh. This calculation shows that the relative volume of NOM is considerable. The calculated volume ratio can be transformed into an average mass density (ρ) of the NOM–oxide association being close to $\rho \sim 1700 \pm 100$ kg/m^3 particles. The calculated mass density refers to oxide particles in our soils with the average specific surface area. However, at a given NOM loading per unit surface area (mg NOM/m^2), a variation in the particle size will lead to a range of mass densities of the NOM–oxide association. Increase of the oxide particle size will lead to an increase of the mass density of the NOM–oxide association. For instance, in case of a specific surface area of 300 m^2/g for the natural (hydr)oxide particles, the calculated mass density of the mineral–NOM association will be $\rho \sim 2000$ kg/m^3 particles. A comparable number is calculated for synthetic ferrihydrite (Fh) with a maximum loading of organic carbon of 320 mg OC/g Fh or 720 mg NOM/g Fh (Kaiser et al., 2007), having a volume ratio NOM/Fh of ~ 2 m^3 NOM/m^3 Fh. On the other hand, the presence of larger molecules like humin ($M \sim 100{,}000$ Da, $d \sim 10$ nm) will decrease the mass density of the micro-aggregates if present. In addition, the mass density will be lowered due to the presence of Al as a light element in the natural oxide fraction compared to Fe. The above-calculated mass densities are typical numbers for the heavy density fractions of natural organic matter in soils (Christensen, 1992; Wagai et al., 2008). These fractions are generally considered as more refractorily in terms of microbial decomposition and can be very dominant (>80–90%) in soils (Wagai et al., 2008).

In Fig. 7b, the oxide–NOM association is schematically depicted as a combination of attached but rather separate particles. Actually, the ensemble of individual organic molecules (FA, HA, and humin) may interact with each other partly forming intertwined structures, enforced by hydrophobic effects, metal-ion- and H-bridging. These binding mechanisms may support the incorporation of additional organic matter in the NOM–mineral nanoparticles of the micro-aggregates, depending on the soil conditions regulating the input and output of organic matter at the system level. The presence of organic matter above a monolayer coverage of $\sim$1–2 mg OC/m^2 is found for a number of our soils (Fig. 7a) and in literature. The incorporation of additional carbon in the oxide–NOM nanoparticle association is effectively similar to a multilayer adsorption of variety of NOM molecules in the NOM–oxide association. This will decrease the mass density of the NOM–oxide association. Of course, formation of coagulated organic matter will also lead to a carbon loading above a monolayer level. This coagulated fraction is considered as true light-density organic matter. The light-density fraction either true or mineral-associated is often quite limited in extent (Wagai et al., 2008). The high-density fraction usually dominates and may have a significantly lower higher C/N ratio, which may point to microbial-processed organic matter (Wagai et al., 2008) in the mineral–NOM association.

It is remarkable that a large number of the agricultural soils has a surprisingly low loading when scaled per unit effective surface area. We may speculate that this is due to the rather intense use of these soils with favorable conditions for microbial degradation of organic matter, such as the quality of the organic matter, the availability of nutrients in particular nitrogen, and pH. In addition, temperature, the physical accessibility, the soil moisture content, and the presence of sufficient oxygen are important factors. The present methodology to derive an effective surface area, allowing new scaling of NOM, may contribute to an improvement of the understanding of these factors as regulators of the dynamics of natural organic matter in soil. In addition, the present methodology to derive the effective surface area may improve our understanding of soil formation.

The embedding of oxide particles in a matrix of NOM (Fig. 7b) may (partly) explain the slow adsorption kinetics of PO_4 that is often observed in experiments with soil. For adsorption, the phosphate ions have to penetrate into a negatively charged gel-like matrix (Fig. 7b) from which these ions are excluded electrostatically. Moreover, the final adsorption of PO_4 may require desorption of NOM which may also be a rather slow process.

At a given adsorption of NOM, its chemical interaction with the surface groups of the (hydr)oxide by ligand exchange (Fig. 7c) can be variable. The surface interaction depends on the profile of the electrostatic potential in the inner Stern layer, which is determined by the collective presence of e.g. protons, phosphate, and NOM ligands. This mutual interaction can be handled with the LCD model (Weng et al., 2008). In part II (Hiemstra et al., 2010), we will discuss a straightforward strategy to implement in a simplified manner the effect of interfacial NOM in the CD model.

5. CONCLUSIONS

- The equilibration of natural samples using 0.5 M sodium bicarbonate (pH = 8.5) solution and an excess amount of activated carbon reduces the complexity of these systems in terms of modeling compared to natural multi-component conditions. The high concentration of the added competitor (HCO_3^- ions) enables a fast penetration into natural porous oxides, desorption of phosphate, and equilibration at internal and external surfaces, reaching a (semi)-equilibrium in about 10–15 days.
- The competitive phosphate–carbonate behavior is determined by the interfacial charge distribution (CD) of the various surface species. This behavior enables the description of the HCO_3^- concentration dependency of the phosphate adsorption and the effect of a changing solid–solution ratio in natural samples by choosing only an effective reactive surface area and a fraction of reversibly adsorbed phosphate.
- The effective reactive surface area (A) on our top soils ranges between $A \sim 3$ and ~ 30 m^2/g sample and is not very well correlated with the amount of Fe and Al oxide extracted with oxalate or DCB. The effective specific surface area (SSA) of the natural oxide fraction, scaled on the total iron and aluminum (hydr)oxide (DCB) content, is mostly between SSA $\sim$200 and $\sim$1200 m^2/g oxide and the corresponding spherical particle size is between $\sim$1 and 10 nm.
- In the set of mineral soils studied, a strong correlation exists between the natural oxide fraction and natural organic matter. For many non-clay soils, the NOM loading is about 1.4 ± 0.2 mg OC/m^2, equivalent with a monolayer thickness of about 2.0 ± 0.3 nm. The observed relationship suggests the formation of a NOM–oxide nanoparticle association. The calculated average NOM volume in such micro-aggregates is $\sim$80% and the mass density is about 1700 kg/m^3, a typical value for the high-density organic matter fraction. Only a fraction of the total amount of organic matter associated with the oxide particles is active in the competition with phosphate that mainly takes place in the inner Stern layer near the surface.
- For the top soils studied, the variation in the reversible phosphate loading is unusually large ($\Gamma = \sim$1–3 μmol/m^2) considering the limited variation in the phosphate concentrations and pH and the shape of the high-affinity isotherm. The large natural variation is supposed to be due to the interaction of NOM as will be discussed in part II of this series.

ACKNOWLEDGMENTS

We greatly appreciate the comments and questions of our reviewers. We also like to thank the Associate Editor. We highly appreciate the financial support of the EU, funding project FUNMIG (516514, F16W-2004).

APPENDIX A

Table A. Aqueous speciation reactions and their equilibrium constants ($I = 0$).

Species	Reaction	log K
HPO_4^{2-}	$PO_4^{3-} + 1H^+ \iff HPO_4^{2-}$	12.35[a]
$H_2PO_4^-$	$PO_4^{3-} + 2H^+ \iff H_2PO_4^-$	19.55[a]
$H_3PO_4^0$	$PO_4^{3-} + 3H^+ \iff H_3PO_4^0$	21.70[a]
$NaPO_4^{2-}$	$PO_4^{3-} + 1Na^+ \iff NaPO_4^{2-}$	2.05[b]
$NaHPO_4^-$	$PO_4^{3-} + 1H^+ + 1Na^+ \iff NaHPO_4^-$	13.4[a,b]
$CaPO_4^-$	$PO_4^{3-} + 1Ca^{2+} \iff CaPO_4^-$	6.46[a]
$CaHPO_4^0$	$PO_4^{3-} + 1H^+ + 1Ca^{2+} \iff CaHPO_4^0$	15.09[a]
$CaH_2PO_4^+$	$PO_4^{3-} + 2H^+ + 1Ca^{2+} \iff CaH_2PO_4^+$	20.95[a]
HCO_3^-	$CO_3^{2-} + 1H^+ \iff HCO_3^-$	10.33[a]
$H_2CO_3^*$	$CO_3^{2-} + 2H^+ \iff H_2CO_3^*$	16.69[a]
CO_2(g)	$CO_3^{2-} + 2H^+ \iff H_2O(l) + CO_2$ (g)	18.15[a]
$NaHCO_3^0$	$CO_3^{2-} + 1Na^+ + 1H^+ \iff NaHCO_3^0$	10.14[c]
$NaCO_3^-$	$CO_3^{2-} + 1Na^+ \iff NaCO_3^-$	1.02[c]
$Na_2CO_3^0$	$CO_3^{2-} + 2Na^+ \iff Na_2CO_3^0$	0.01[a]
$CaHCO_3^+$	$CO_3^{2-} + 1H^+ + 1Ca^{2+} \iff CaHCO_3^+$	11.45[a]
$CaCO_3^0$	$CO_3^{2-} + 1Ca^{2+} \iff CaCO_3^0$	3.14[a]
$CaCl^+$	$Ca^{2+} + 1Cl^- \iff CaCl^+$	−1.0[a]
$CaCl_2^0$	$Ca^{2+} + 2Cl^- \iff CaCl_2^0$	0.0[a]
$NaCl^0$	$Na^+ + Cl^- \iff NaCl^0$	−0.80[d]
$NaNO_3^0$	$Na^+ + NO_3^- \iff NaNO_3^0$	−0.60[e]
H_2O(l)	$H^+ + OH^- \iff H_2O$(l)	14.00[e]

[a]From Lindsay (1979).
[b]From Rahnemaie et al. (2007b).
[c]From Millero and Schreiber (1982).
[d]From Sverjensky et al. (1997).
[e]From Smith and Martell (1981).

REFERENCES

Ali M. A. and Dzombak D. A. (1996) Competitive sorption of simple organic acids and sulfate on goethite. *Environ. Sci. Technol.* **30**, 1061–1071.

Antelo J., Avena M., Fiol S., Lopez R. and Arce F. (2005) Effects of pH and ionic strength on the adsorption of phosphate and arsenate at the goethite–water interface. *J. Colloid Interf. Sci.* **285**(2), 476–486.

Antelo J., Arce F., Avena M., Fiol S., López R. and Macías F. (2007) Adsorption of a soil humic acid at the surface of goethite

and its competitive interaction with phosphate. *Geoderma* **138**(1–2), 12–19.

Bargar J. R., Kubicki J. D., Reitmeyer R. and Davis J. A. (2005) ATR-FTIR spectroscopic characterization of coexisting carbonate surface complexes on hematite. *Geochim. Cosmochim. Acta* **69**(6), 1527–1542.

Barrow N. J. and Shaw T. C. (1975) Slow Reactions between soil and anions. 5. Effects of period of prior contact on desorption of phosphate from soils. *Soil Sci.* **119**(4), 311–320.

Barrow N. J. and Shaw T. C. (1976a) Sodium bicarbonate as an extractant for soil phosphate, I. Separation of the factors affecting the amount of phosphate displaced from soil from those affecting secondary adsorption. *Geoderma* **16**(2), 91–107.

Barrow N. J. and Shaw T. C. (1976b) Sodium bicarbonate as an extractant for soil phosphate, II. Effect of varying the conditions of extraction on the amount of phosphate initially displaced and on the secondary adsorption. *Geoderma* **16**(2), 109–123.

Barrow N. J., Bowden J. W., Posner A. M. and Quirk J. P. (1980) Describing the effects of electrolyte on adsorption of phosphate by a variable charge surface. *Aust. J. Soil Res.* **18**(4), 395–404.

Boily J.-F. (1999) *The Surface Complexation of Ions at the Goethite (a-FeOOH)/Water Interface: a Multisite Complexation Approach*. Umeå University.

Brecevic L. and Kralj D. (2007) On calcium carbonates: from fundamental research to application. *Croat. Chem. Acta* **80**(3–4), 467–484.

Cances B., Ponthieu M., Castrec-Rouelle M., Aubry E. and Benedetti M. F. (2003) Metal ions speciation in a soil and its solution: experimental data and model results. *Geoderma* **113**(3–4), 341–355.

Christensen B. T. (1992) Physical fractionation of soil and organic matter in primary particle size and density separates. *Adv. Soil Sci.* **20**, 1–90.

Christl I. and Kretzschmar R. (1999) Competitive sorption of copper and lead at the oxide–water interface: implications for surface site density. *Geochim. Cosmoschim. Acta* **63**(19–20), 2929–2938.

Cihacek L. J. and Bremner J. M. (1979) Simplified ethylene-glycol monoethyl ether procedure for assessment of soil surface-area. *Soil Sci. Soc. Am. J.* **43**(4), 821–822.

Coffin D. E. (1963) A method for the determination of free iron in soils and clays. *Can. J. Soil Sci.* **43**, 7–17.

Cornell R. M. and Schwertmann U. (1996) *The Iron Oxides: Structures, Properties, Reactions, Occurrence and Uses*. VCH.

Criscenti L. J. and Sverjensky D. A. (1999) The role of electrolyte anions (ClO_4^-, NO_3^-, and Cl^-) in divalent metal (M^{2+}) adsorption on oxide and hydroxide surfaces in salt solution. *Am. J. Sci.* **299**, 828–899.

Davis J. A. and Leckie J. O. (1978) Surface ionization and complexation at the oxide/water interface. II Surface properties of amorphous iron oxyhydroxide and adsorption of metal ions. *J. Colloid Interf. Sci.* **67**, 90–105.

Davis J. A., James R. and Leckie J. O. (1978) Surface ionization and complexation at the oxide/water interface. I. Computation of electrical double layer properties in simple electrolytes. *J. Colloid Interf. Sci.* **63**, 480–499.

Dijkstra J. J., Meeussen J. C. L. and Comans R. N. J. (2004) Leaching of heavy metals from contaminated soils: an experimental and modeling study. *Environ. Sci. Technol.* **38**(16), 4390–4395.

Dzombak D. A. and Morel F. M. M. (1990) *Surface Complexation Modeling: Hydrous Ferric Oxide*. John Wiley & Sons, New York,, p. 393.

Eusterhues K., Rumpel C., Kleber M. and Kogel-Knabner I. (2003) Stabilisation of soil organic matter by interactions with minerals as revealed by mineral dissolution and oxidative degradation. *Org. Geochem.* **34**(12), 1591–1600.

Eusterhues K., Rumpel C. and Kogel-Knabner I. (2005) Organo-mineral associations in sandy acid forest soils: importance of specific surface area, iron oxides and micropores. *Eur. J. Soil Sci.* **56**(6), 753–763.

Eusterhues K., Wagner F. E., Hausler W., Hanzlik M., Knicker H., Totsche K. U., Kogel-Knabner I. and Schwertmann U. (2008) Characterization of ferrihydrite–soil organic matter coprecipitates by X-ray diffraction and Mossbauer spectroscopy. *Environ. Sci. Technol.* **42**(21), 7891–7897.

Filius J. D., Hiemstra T. and Van Riemsdijk W. H. (2000) Adsorption of fulvic acid on goethite. *Geochim. Cosmochim. Acta* **64**(1), 51–60.

Fukushi K. and Sato T. (2005) Using a surface complexation model to predict the mature and stability of nanoparticles. *Environ. Sci. Technol.* **39**(5), 1250–1256.

Goldberg S., Lesch S. M. and Suarez D. L. (2002) Predicting molybdenum adsorption by soils using soil chemical. Parameters in the constant capacitance model. *Soil Sci. Soc. Am. J.* **66**(6), 1836–1842.

Griffioen J. (2006) Extent of immobilisation of phosphate during aeration of nutrient-rich, anoxic groundwater. *J. Hydrol.* **320**(3–4), 359–369.

Gu B. H., Schmitt J., Chen Z. H., Liang L. Y. and McCarthy J. F. (1994) Adsorption and desorption of natural organic-matter on iron-oxide – mechanisms and models. *Environ. Sci. Technol.* **28**(1), 38–46.

Gu B. H., Mehlhorn T. L., Liang L. Y. and McCarthy J. F. (1996) Competitive adsorption, displacement, and transport of organic matter on iron oxide. 1. Competitive adsorption. *Geochim. Cosmoschim. Acta* **60**(11), 1943–1950.

Gustafsson J. P. (2001) Modelling competitive anion adsorption on oxide minerals and an allophane-containing soil. *Eur. J. Soil Sci.* **52**(4), 639–653.

Hassellov M. and Von der Kammer F. (2008) Iron oxide as geochemical nanovectors for metal transport in soil–river systems. *Elements* **4**, 401–406.

Hiemstra T. and Van Riemsdijk W. H. (1996) A surface structural approach to ion adsorption: the charge distribution (CD) model. *J. Colloid Interf. Sci.* **179**, 488–508.

Hiemstra T. and Van Riemsdijk W. H. (1999) Surface structural ion adsorption modeling of competitive binding of oxyanions by metal (hydr)oxides. *J. Colloid Interf. Sci.* **210**, 182–193.

Hiemstra T. and Van Riemsdijk W. H. (2006) On the relationship between charge distribution, surface hydration and the structure of the interface of metal hydroxides. *J. Colloid Interf. Sci.* **301**, 1–18.

Hiemstra T. and Van Riemsdijk W. H. (2007) Surface complexation of selenite on goethite: MO/DFT geometry and charge distribution. *Croat. Chem. Acta* **80**(3–4), 313–324.

Hiemstra T. and Van Riemsdijk W. H. (2009) A surface structural model for ferrihydrite I: sites related to primary charge, molar mass, and mass density. *Geochim. Cosmochim. Acta* **73**, 4423–4436.

Hiemstra T., Venema P. and Van Riemsdijk W. H. (1996) Intrinsic proton affinity of reactive surface groups of metal (hydr)oxides: the bond valence principle. *J. Colloid Interf. Sci.* **184**, 680–692.

Hiemstra T., Rahnemaie R. and Van Riemsdijk W. H. (2004) Surface complexation of carbonate on goethite: IR spectroscopy, structure and charge distribution. *J. Colloid Interf. Sci.* **278**, 282–290.

Hiemstra T., Barnett M. O. and Van Riemsdijk W. H. (2007) Interaction of silicic acid with goethite. *J. Colloid Interf. Sci.* **310**, 8–17.

Hiemstra T., Antelo J., Van Rotterdam A. M. D. and Van Riemsdijk W. H. (2010) Nanoparticles in natural systems II: the natural oxide fraction at interaction with natural organic matter and phosphate. *Geochim. Cosmoschim. Acta* **74**(1), 59–69.

Hingston F. J., Posner A. M. and Quirk J. P. (1968) Adsorption of selenite by goethite. In Symposium on Adsorption from Aqueous Solution Advances in Chemical Series, vol. 70. pp. 82–90.

Holmgren G. G. (1967) A rapid citrate–dithionite extractable iron procedure. *Soil Sci. Soc. Am. Proc.* **31**(2), 210.

Hyacinthe C. and Van Cappellen P. (2004) An authigenic iron phosphate phase in estuarine sediments: composition, formation and chemical reactivity. *Mar. Chem.* **91**(1–4), 227–251.

Janney D. E., Cowley J. M. and Buseck P. R. (2000) Transmission electron microscopy of synthetic 2- and 6-line ferrihydrite. *Clays Clay Miner.* **48**(1), 111–119.

Kaiser K. and Guggenberger G. (2000) The role of DOM sorption to mineral surfaces in the preservation of organic matter in soils. *Org. Geochem.* **31**(7–8), 711–725.

Kaiser K. and Guggenberger G. (2003) Mineral surfaces and soil organic matter. *Eur. J. Soil Sci.* **54**(2), 219–236.

Kaiser K., Mikutta R. and Guggenberger G. (2007) Increased stability of organic matter sorbed to ferrihydrite and goethite on aging. *Soil Sci. Soc. Am. J.* **71**(3), 711–719.

Keil R. G., Montlucon D. B., Prahl F. G. and Hedges J. I. (1994) Sorptive preservation of labile organic-matter in marine-sediments. *Nature* **370**(6490), 549–552.

Keizer M. G. and Van Riemsdijk W. H. (1998) *ECOSAT, Equilibrium Calculation of Speciation and Transport. Technical Report Department Soil Quality*. Wageningen University.

Kennedy M. J., Pevear D. R. and Hill R. J. (2002) Mineral surface control of organic carbon in black shale. *Science* **295**(5555), 657–660.

Kinniburgh D. G. (1993) Fit, Technical Report WD/93/23. British Geological Survey.

Koopmans G. F., Chardon W. J., de Willigen P. and van Riemsdijk W. H. (2004) Phosphorus desorption dynamics in soil and the link to a dynamic concept of bioavailability. *J. Environ. Qual.* **33**(4), 1393–1402.

Kostka J. E. and Luther G. W. (1994) Partitioning and speciation of solid-phase iron in salt-marsh sediments. *Geochim. Cosmoschim. Acta* **58**(7), 1701–1710.

Lienemann C. P., Monnerat M., Dominik J. and Perret D. (1999) Identification of stoichiometric iron–phosphorus colloids produced in a eutrophic lake. *Aquat.1 Sci.* **61**(2), 133–149.

Lindsay W. L. (1979) *Chemical Equilibria in Soils*. Wiley-Interscience.

Lofts S. and Tipping E. (1998) An assemblage model for cation binding by natural particulate matter. *Geochim. Cosmoschim. Acta* **62**(15), 2609–2625.

Logue B. A., Smith R. W. and Westall J. C. (2004) U(VI) adsorption on natural iron-coated sands: comparison of approaches for modeling adsorption on heterogeneous environmental materials. *Appl. Geochem.* **19**(12), 1937–1951.

Luengo C., Brigante M., Antelo J. and Avena M. (2006) Kinetics of phosphate adsorption on goethite: comparing batch adsorption and ATR-IR measurements. *J. Colloid Interf. Sci.* **300**(2), 511–518.

Lumsdon D. G. (2004) Partitioning of organic carbon, aluminium and cadmium between solid and solution in soils: application of a mineral-humic particle additivity model. *Eur. J. Soil Sci* **55**(2), 271–285.

Lutzenkirchen J. (2004) Modelling uranyl adsorption to quartz – application of the CD-MUSIC concept. *Geochim. Cosmoschim. Acta* **68**(11), A502.

Mayer L. M. (1994) Surface-area control of organic-carbon accumulation in continental-shelf sediments. *Geochim. Cosmoschim. Acta* **58**(4), 1271–1284.

Mehra O. P. and Jackson M. L. (1960) Iron oxide removal from the soils and clays by dithionite–citrate system buffered with sodium bicarbonate. *Clays Clay Miner.* **7**, 317–327.

Meima J. A. and Comans R. N. J. (1998) Application of surface complexation precipitation modeling to contaminant leaching from weathered municipal solid waste incinerator bottom ash. *Environ. Sci. Technol.* **32**(5), 688–693.

Millero F. J. and Schreiber D. R. (1982) Activity coefficients of the ionic components of natural water. *Am. J. Sci.* **282**, 1508–1540.

Mödl C., Wörmann H. and Amelung W. (2007) Contrasting effects of different types of organic material on surface area and microaggregation of goethite. *Geoderma* **141**(3–4), 167–173.

Murphy P. J., Posner A. M. and Quirk J. P. (1976) Characterization of partially neutralized ferric nitrate solutions. *J. Colloid Interf. Sci.* **56**(2), 270–283.

Olsen S. R., Cole C. V., Watanabe F. S. and Dean L. A. (1954). , pp. 1–19.

Parks G. A. and De Bruyn P. L. (1962) The zero point of charge of oxides. *J. Phys. Chem.* **66**, 967–973.

Ponthieu M., Juillot F., Hiemstra T., van Riemsdijk W. H. and Benedetti M. F. (2006) Metal ion binding to iron oxides. *Geochim. Cosmoschim. Acta* **70**(11), 2679–2698.

Rahnemaie R., Hiemstra T. and Van Riemsdijk W. H. (2006) A new structural approach for outersphere complexation, tracing the location of electrolyte ions. *J. Colloid Interf. Sci.* **293**, 312–321.

Rahnemaie R., Hiemstra T. and Van Riemsdijk W. H. (2007a) Carbonate adsorption on goethite in competition with phosphate. *J. Colloid Interf. Sci.* **315**(2), 415–425.

Rahnemaie R., Hiemstra T. and Van Riemsdijk W. H. (2007b) Geometry, charge distribution and surface speciation of phosphate on goethite. *Langmuir* **23**, 3680–3689.

Rietra R. P. J. J., Hiemstra T. and Van Riemsdijk W. H. (1999) The relationship between molecular structure and ion adsorption on variable charge minerals. *Geochim. Cosmochim. Acta* **63**(19/20), 3009–3015.

Rietra R. P. J. J., Hiemstra T. and Van Riemsdijk W. H. (2001) Interaction of calcium and phosphate adsorption on goethite. *Environ. Sci. Technol.* **35**, 3369–3374.

Roden E. E. and Zachara J. M. (1996) Microbial reduction of crystalline iron(III) oxides: influence of oxide surface area and potential for cell growth. *Environ. Sci. Technol.* **30**(5), 1618–1628.

Rosentreter J. J., Swantje Quarder H., Smith R. W. and McLing T. (1998) Uranium sorption onto natural sands as a function of sediment characteristics and solution pH. In *Adsorption of Metals by Geomedia* (ed. E. A. Jenne). Academic Press.

Schroder T. J., Hiemstra T., Vink J. P. M. and van der Zee S. (2005) Modeling of the solid–solution partitioning of heavy metals and arsenic in embanked flood plain soils of the rivers Rhine and Meuse. *Environ. Sci. Technol.* **39**(18), 7176–7184.

Schulten H. R. and Leinweber P. (2000) New insights into organic-mineral particles: composition, properties and models of molecular structure. *Biol. Fert. Soils* **30**(5–6), 399–432.

Schwertmann U. (1973) Use of oxalate for Fe extraction from soils. *Can. J. Soil Sci.* **53**(2), 244–246.

Schwertmann U. and Fischer W. R. (1973) Natural amorphous ferric hydroxide. *Geoderma* **10**(3), 237–247.

Smith R. M. and Martell A. E. (1981) *Critical Stability Constants*. Plenum.

Stachowicz M., Hiemstra T. and van Riemsdijk W. H. (2008) Multi-competitive interaction of As(III) and As(V) oxyanions

with Ca^{2+}, Mg^{2+}, PO_4^{3-}, and CO_3^{2-} ions on goethite. *J. Colloid Interf. Sci.* **320**(2), 400–414.

Stern O. (1924) Zur theory der electrolytischen doppelschicht. *Z. Electrochem.* **30**, 508–516.

Strauss R., Brummer G. W. and Barrow N. J. (1997) Effects of crystallinity of goethite. 2. Rates of sorption and desorption of phosphate. *Eur. J. Soil Sci.* **48**(1), 101–114.

Sverjensky D. A. (2005) Prediction of surface charge on oxides in salt solutions: revisions for 1:1 (M^+L^-) electrolytes. *Geochim. Cosmochim. Acta* **69**(2), 225–257.

Sverjensky D. A., Shock E. L. and Helgeson H. C. (1997) Prediction of the thermodynamic properties of aqueous metal complexes to 1000 °C and 5 kb. *Geochim. Cosmoschim. Acta* **61**(7), 1359–1412.

Tadanier C. J. and Eick M. J. (2002) Formulating the charge-distribution multisite surface complexation model using FITEQL. *Soil Sci. Soc. Am. J.* **66**(5), 1505–1517.

Tejedor-Tejedor M. I. and Anderson M. A. (1990) Protonation of phosphate on the surface of goethite as studied by CIR-FTIR and electrophoretic mobility. *Langmuir* **6**, 602–611.

Thompson A., Chadwick O. A., Rancourt D. G. and Chorover J. (2006) Iron-oxide crystallinity increases during soil redox oscillations. *Geochim. Cosmoschim. Acta* **70**(7), 1710–1727.

Torn M. S., Trumbore S. E., Chadwick O. A., Vitousek P. M. and Hendricks D. M. (1997) Mineral control of soil organic carbon storage and turnover. *Nature* **389**(6647), 170–173.

Torrent J., Barron V. and Schwertmann U. (1990) Phosphate adsorption and desorption by goethites differing in crystal morphology. *Soil Sci. Soc. Am. J.* **54**, 1007–1012.

Torrent J., Schwertmann U. and Barron V. (1992) Fast and slow phosphate sorption by goethite-rich natural materials. *Clays Clay Miner.* **40**(1), 14–21.

van der Zee C., Roberts D. R., Rancourt D. G. and Slomp C. P. (2003) Nanogoethite is the dominant reactive oxyhydroxide phase in lake and marine sediments. *Geology* **31**(11), 993–996.

van Erp P. J., Houba V. J. G. and Van Beusichem M. L. (1998) One hundredth molar calcium chloride extraction procedure. Part I: a review of soil chemical, analytical, and plant nutritional aspects. *Commun. Soil Sci. Plan.* **29**(11–14), 1603–1623.

Vanderzee S. and Vanriemsdijk W. H. (1988) Model for long-term phosphate reaction-kinetics in soil. *J. Environ. Qual.* **17**(1), 35–41.

Voegelin A., Vulava V. M. and Kretzschmar R. (2001) Reaction-based model describing competitive sorption and transport of Cd, Zn, and Ni in an acidic soil. *Environ. Sci. Technol.* **35**(8), 1651–1657.

Wada K. (1989) Allophane and imogolite. In *Minerals in Soil Environment* (eds. J. B. Dixon and S. B. Weed). Soil Science Society of America, pp. 1051–1087.

Wagai R. and Mayer L. M. (2007) Sorptive stabilization of organic matter in soils by hydrous iron oxides. *Geochim. Cosmoschim. Acta* **71**(1), 25–35.

Wagai R., Mayer L. M., Kitayama K. and Knicker H. (2008) Climate and parent material controls on organic matter storage in surface soils: a three-pool, density-separation approach. *Geoderma* **147**(1–2), 23–33.

Wagai R., Mayer L. M. and Kitayama K. (2009) Extent and nature of organic coverage of soil mineral surfaces assessed by a gas sorption approach. *Geoderma* **149**(1–2), 152–160.

Walker T. W. and Syers J. K. (1976) Fate of phosphorus during pedogenesis. *Geoderma* **15**(1), 1–19.

Weng L. P., Temminghoff E. J. M. and van Riemsdijk W. H. (2001) Contribution of individual sorbents to the control of heavy metal activity in sandy soil. *Environ. Sci. Technol.* **35**(22), 4436–4443.

Weng L. P., Van Riemsdijk W. H. and Hiemstra T. (2006) Adsorption free energy of variable-charge nanoparticles to a charged surface in relation to the change of the average chemical state of the particles. *Langmuir* **22**(1), 389–397.

Weng L. P., Van Riemsdijk W. H. and Hiemstra T. (2007) Adsorption of humic acids onto goethite: effects of molar mass, pH and ionic strength. *J. Colloid Interf. Sci.* **314**(1), 107–118.

Weng L. P., Van Riemsdijk W. H. and Hiemstra T. (2008) Humic nano-particles at the oxide–water interface: interaction with phosphate ion adsorption. *Environ. Sci. Technol.* **42**(23), 8747–8752.

Westall J. and Hohl H. (1980) A comparison of electrostatic models for the oxide/solution interface. *Adv. Colloid Interf. Sci.* **12**, 265–294.

Wiseman C. L. S. and Puttmann W. (2006) Interactions between mineral phases in the preservation of soil organic matter. *Geoderma* **134**(1–2), 109–118.

Wolthoorn A., Temminghoff E. J. M., Weng L. P. and van Riemsdijk W. H. (2004) Colloid formation in groundwater: effect of phosphate, manganese, silicate and dissolved organic matter on the dynamic heterogeneous oxidation of ferrous iron. *Appl. Geochem.* **19**(4), 611–622.

Zhou Q. H., Maurice P. A. and Cabaniss S. E. (2001) Size fractionation upon adsorption of fulvic acid on goethite: equilibrium and kinetic studies. *Geochim. Cosmoschim. Acta* **65**(5), 803–812.

Associate editor: Stephan M. Kraemer